

1 Marine and terrestrial environmental changes in NW  
2 Europe preceding carbon release at the Paleocene-Eocene  
3 transition

4  
5

6 Sev Kender<sup>a,\*</sup>

7 Michael H. Stephenson<sup>a</sup>

8 James B. Riding<sup>a</sup>

9 Melanie J. Leng<sup>b,c</sup>

10 Robert W. O'B. Knox<sup>a</sup>

11 Victoria L. Peck<sup>d</sup>

12 Christopher P. Kendrick<sup>b</sup>

13 Michael A. Ellis<sup>a</sup>

14 Christopher H. Vane<sup>a</sup>

15 Rachel Jamieson<sup>e</sup>

16  
17

18 <sup>a</sup> *British Geological Survey, Nottingham, NG12 5GG, UK*

19 <sup>b</sup> *NERC Isotope Geosciences Laboratory, British Geological Survey, Nottingham, NG12 5GG, UK*

20 <sup>c</sup> *Department of Geology, University of Leicester, Leicester LE1 7RH, UK*

21 <sup>d</sup> *British Antarctic Survey, High Cross, Madingley Road, Cambridge, CB3 0ET, UK*

22 <sup>e</sup> *School of Geosciences, University of Edinburgh, Edinburgh, EH9 3JW, UK*

23  
24

25 \* Corresponding author.

26 *E-mail address: sev.kender@bgs.ac.uk (S. Kender)*

27

28 ABSTRACT

29

30 Environmental changes associated with the Paleocene-Eocene Thermal Maximum (PETM, ~56 Ma)  
31 have not yet been documented in detail from the North Sea Basin. Located within proximity to the  
32 North Atlantic Igneous Province (NAIP), the Kilda Basin, and the northern rain belt (paleolatitude  
33 ~54°N) during the PETM, this is a critical region for testing proposed triggers of atmospheric  
34 carbon release that may have caused the global negative  $\delta^{13}\text{C}$  carbon isotope excursion (CIE) in  
35 marine and terrestrial environments. The CIE onset is identified from organic matter  $\delta^{13}\text{C}$  in  
36 exceptional detail within a highly expanded sedimentary sequence. Pollen and spore assemblages  
37 analysed in the same samples for the first time allow a reconstruction of possible changes to  
38 vegetation on the surrounding landmass. Multiproxy palynological, geochemical, and  
39 sedimentologic records demonstrate enhanced halocline stratification and terrigenous deposition  
40 well before ( $10^3$  yrs) the CIE, interpreted as due to either tectonic uplift possibly from a nearby  
41 magmatic intrusion, or increased precipitation and fluvial runoff possibly from an enhanced  
42 hydrologic cycle. Stratification and terrigenous deposition increased further at the onset and within  
43 the earliest CIE which, coupled with evidence for sea level rise, may be interpreted as an increase in  
44 precipitation over NW Europe consistent with an enhanced hydrologic cycle in response to global  
45 warming during the PETM. Palynological evidence indicates a flora dominated by pollen from  
46 coastal swamp conifers before the CIE was abruptly replaced with a more diverse assemblage of  
47 generalist species including pollen similar to modern alder, fern and fungal spores. This may have  
48 resulted from flooding of coastal areas due to relative sea level rise, and/or ecological changes  
49 forced by climate. A shift towards more diverse angiosperm and pteridophyte vegetation within the  
50 early CIE, including pollen similar to modern hickory, documents a long term change to regional  
51 vegetation.

52

53 *Keywords:*

54 Paleocene-Eocene boundary

55 PETM

56 carbon isotope excursion

57 paleoecology

58 paleoceanography

59 North Sea

60

## 61 **1. Introduction**

62

63 The PETM was a period of geologically-rapid global warming that punctuated a warming  
64 Eocene climate ~55.8 Ma ago (Charles et al., 2011), and saw sea surface temperatures rise by ~5–  
65 8°C from background levels (Zachos et al., 2005; Sluijs et al., 2007). It was associated with a  
66 substantial injection of  $\delta^{13}\text{C}$ -depleted carbon into the ocean-atmosphere system (see Pagani et al.,  
67 2006a) over <20 ka (Cui et al., 2011), causing a negative carbon isotope excursion (CIE) of  
68 between –2 and –7‰ in marine and terrestrial sediments (see overview in Schouten et al., 2007)  
69 lasting ~170 ka (Röhl et al., 2007), and a prominent dissolution horizon in the deep sea signifying  
70 deep ocean acidification (Kennett and Stott 1991; Zachos et al., 2005). The source and rate of  
71 released carbon is still under debate (Pagani et al., 2006a; Zeebe et al., 2009; Cui et al., 2011), but  
72 may have been linked to the dissociation of marine hydrates containing biogenic methane ( $\delta^{13}\text{C}$  of <  
73 –60 ‰) (Dickens et al., 1995), thermogenic methane from marine sediments around the Norwegian  
74 Sea (Svensen et al., 2004), or dissolved methane from a silled Kilda Basin between Greenland and  
75 Norway (Nisbet et al., 2009).

76 The PETM may be a good analogue to test modelling studies that suggest current global  
77 warming trends may result in an enhanced hydrologic cycle (Seager et al., 2010), whereby  
78 increased precipitation in temperate rain belts is coupled with increased evaporation in lower  
79 latitudes. Modelling studies of the PETM have further indicated the potential importance of an  
80 increased hydrologic cycle (Lunt et al., 2010; Bice and Marotzke 2002), which could have altered  
81 ocean circulation causing methane hydrate reservoirs to destabilise, triggering massive carbon  
82 release (Bice and Marotzke, 2002). Palynological evidence from Arctic Spitsbergen (Harding et al.,  
83 2011) and New Zealand (Crouch et al., 2003a) suggests increased terrestrial runoff occurred at the  
84 onset of the CIE which may be related to hydrologic changes, and massive Pyrenees conglomerate  
85 deposits have been interpreted as the result of an abrupt increase in extreme precipitation within the  
86 early CIE (Schmitz and Pujalte, 2007). In addition hydrogen and carbon isotope measurements of  
87 terrestrial plant and aquatic-derived *n*-alkanes from the central Arctic Ocean indicate that the core  
88 of the PETM was associated with increased precipitation and hence hydrologic cycle (Pagani et al.,  
89 2006b), although the onset of PETM warming was not recovered in the sediment core. Despite  
90 numerous additional evidence for changes in terrestrial runoff and potentially hydrology during the  
91 PETM (see overview in McInterney and Wing, 2011), there is a lack of clear evidence for  
92 hydrologic changes from high resolution sections able to resolve important lead/lag relationships,  
93 and therefore there remains a need for studies of hydrologic changes in sensitive locations over the  
94 onset of the CIE in order to understand the relationship between precipitation and global carbon  
95 release.

96 Biome changes in response to modern global warming have been observed, but approaches  
97 to predict the vulnerability of ecosystems to future changes are still in development (Gonzalez et al.,  
98 2010). Vegetation shifts during the rapid warming associated with the PETM may provide a useful  
99 analogue to future biome responses. Whilst neotropical vegetation in Central America appears to  
100 have responded to warming during the PETM with increased diversity and origination rates  
101 (Jaramillo et al., 2010), central North America experienced a rapid migration of plant communities  
102 associated with lower precipitation at the onset of the CIE (Wing et al., 2005), and southern  
103 England may have experienced a major change in plant composition due to changes in local fire-  
104 regime (Collinson et al., 2009). To better understand biome responses to climatic change during the  
105 PETM, further high resolution vegetation cover studies are needed, specifically from temperate and  
106 boreal forests which may be amongst the most vulnerable ecosystems to global warming (Gonzalez  
107 et al., 2010).

108 In this study we focus on paleoenvironmental signals from a high resolution marine core  
109 collected from the central North Sea (Fig. 1), in order to understand changes to precipitation, ocean  
110 stratification, productivity and vegetation over the onset of the PETM. This core is located in a  
111 critical region proximal to the NAIP, as there are currently no high resolution records of  
112 environmental change during the PETM from the North Sea Basin. Furthermore, as overturning of a  
113 stratified Kilda Basin is hypothesised as a possible trigger for dissolved methane release to the  
114 atmosphere (Nisbet et al., 2009), analysing the stratification history of the nearby North Sea is a  
115 possible way to test this hypothesis.

116

## 117 **2. Regional setting**

118

119 During the late Paleocene–early Eocene the North Sea was a restricted marine basin,  
120 characterised by siliciclastic sedimentation and high terrigenous input, principally from the  
121 Scotland-Faeroe-Shetland landmass (Knox 1998, Fig. S1). Core 22/10a-4 is located in the central  
122 part of the basin (Figs. 1, S1), and is therefore disconnected from many marginal marine processes  
123 that could mask oceanographic signals (e.g. tidal or storm-induced erosion and slumping).  
124 Paleobathymetry estimates in the North Sea during the Paleocene and Eocene are difficult to  
125 constrain accurately, as the extant benthic foraminifera present in the Paleogene are found today  
126 living between 200 and >1000 m water depth (Gradstein et al., 1992), and are controlled  
127 predominantly by substrate and bottom water properties. However using a number of paleoecologic  
128 micropaleontology methods together (Gillmore et al., 2001), along with 2D structural restoration  
129 (Kjennnerud and Sylta 2001), broad agreement was found and central parts of the northern North Sea

130 appear to have had paleodepths of >0.5 km in the earliest Eocene near 22/10a-4 (Kjennerud and  
131 Gillmore, 2003, Fig. S1).

132 As 22/10a-4 is in the deep (>0.5 km) central part of the basin, it acted as a depocentre and  
133 thus exhibits an expanded sedimentary sequence in which we observe no evidence of hiatuses  
134 (erosional surfaces, discontinuous bedding/lamination, truncated isotope stratigraphy). Although  
135 transported material is evident by the thin sandstones (typically <10 cm) interpreted as turbidites,  
136 these have not been sampled in this study. During the late Paleocene, the basin became restricted  
137 following a fall in sea-level of ~100 m that resulted from regional uplift associated with the proto-  
138 Iceland mantle plume in the North Atlantic (see Knox, 1996). This event is evident in 22/10a-4 as a  
139 lithologic change from unbedded to bedded mudstone (the Lista and Sele Formation boundary, Fig.  
140 2). Restriction of the basin also led to the establishment of poorly oxygenated bottom waters, as is  
141 evident by a shift in the benthic foraminiferal assemblages towards low diversity low oxygen-  
142 tolerant agglutinated species (Knox 1996). The CIE at the Paleocene–Eocene boundary was  
143 accompanied by a relative sea level rise, as documented in southeast England (Powell et al., 1996)  
144 and Spitsbergen (Harding et al., 2011), due to the thermal expansion of sea water and possible  
145 melting of ice caps, although the North Sea basin remained restricted as evidenced by the  
146 persistence of low-oxygen facies in 22/10a-4. The North Sea had a widespread freshwater  
147 catchment area, and a halocline was in place from the late Paleocene to early Eocene (Zacke et al.,  
148 2009). Therefore, surface water salinity changes in the North Sea Basin provide a sensitive gauge  
149 for stratification forced by changes in tectonics and the hydrologic cycle.

150

### 151 **3. Methods and materials**

152

#### 153 *3.1. Sedimentology*

154

155 Borehole 22/10a-4 (57°44'8.47''N. 1°50'26.59''E.) comprises a continuous core through the  
156 Forties Sandstone Member and into the Lista Formation (Fig. 2). The core consists of fine grained  
157 shale with interbedded fine to coarse grained sandstone layers interpreted as turbidites, with  
158 occasional mm-thick ash layers (Fig. 3). All samples in this study were taken from claystone  
159 horizons to avoid sampling substantial quantities of transported material. The section of 22/10a-4  
160 analysed in this study is from 2605 m to 2634 m (core depth), chosen because this part of the core is  
161 predominantly in claystone facies and provides a greatly expanded section over the onset of the CIE  
162 (Figs. 2, 3). At ~2609 to 2613 m the claystone becomes finely laminated, with alternately pale and  
163 dark laminae couplets ranging from 1-25 per mm (Fig. S2). The pale laminae consist of clay and

164 fine sand, and the dark laminae are rich in organic carbon and pyrite inclusions. Laminae were  
165 counted at 26 horizons throughout the core and average ~13 pairs per mm.

166

### 167 3.2. *Micropaleontology*

168

169 A total of 71 palynology samples were prepared at the British Geological Survey using  
170 standard preparation procedures (Moore et al., 1991). Samples were demineralized with  
171 hydrochloric (HCl) and hydrofluoric (HF) acids, and residual mineral grains removed using heavy  
172 liquid (zinc bromide) separation. Elvacite was used to mount slides. The palynomorphs were  
173 analysed using a Nikon transmitted light microscope, counting the total number of palynomorphs on  
174 a strew slide (Table S1). Each slide was produced from 1/100<sup>th</sup> of the total material processed,  
175 where the initial weight of material was 5 g of dried sediment. Thus, the palynology counts  
176 represent the total number of specimens per 0.05 g of dried sediment. Statistical analysis was  
177 carried out using the software of Hammer et al. (2005). The %wood/plant tissue was determined by  
178 palynological investigation, and is the sum of ‘%wood plant tissue’ and ‘%various (non-woody)  
179 plant tissue’ in Table S1. Organic material for  $\delta^{13}\text{C}_{\text{AOM}}$  analysis was collected from the same  
180 palynology samples, and the remaining processed material separated into size fractions. The >250  
181  $\mu\text{m}$  fractions, found through light microscope analysis to be dominated (>90%) by amorphous  
182 organic matter (AOM), were also analysed for  $\delta^{13}\text{C}$ . Foraminifera samples of between 20 and 60 g  
183 of dried sediment were processed by washing through a 63  $\mu\text{m}$  sieve with water. All specimens  
184 were counted and converted to foraminifera/g (Table S2). All species exhibited agglutinated (non  
185 calcareous) test walls.

186

### 187 3.3. *Geochemistry*

188

189 All analyses were carried out at the NERC Isotope Geosciences Laboratory. C and N  
190 analyses (from which we present weight % C/N) were performed on 225 samples by combustion in  
191 a Costech ECS4010 Elemental Analyser (EA) calibrated against an Acetanilide standard (Table S3).  
192 C/N atomic ratios were calculated by multiplying by 1.167. Replicate analysis of well-mixed  
193 samples indicated a precision of  $\pm <0.1$ . Carbon isotope analysis was carried out on 289 bulk rock  
194 samples (Table S4) after removing migrated hydrocarbons (Stephenson et al., 2005). The  
195 hydrocarbons were removed by crushing the rock fragments using a ball mill, and the soluble  
196 organic matter from all rock samples was extracted using a Soxhlet extractor. The samples were  
197 refluxed for 24 h in an azeotropic mixture of dichloromethane and methanol (93:7, v/v). All  
198 materials (cellulose Soxhlet thimbles, silica wool, vials) were cleaned with analytical grade organic

199 solvents prior to use. Any remaining solvent was then removed by evaporation and the dried  
200 sediments were transferred to vials. Any calcites (shelly fragments) were removed by placing the  
201 samples in 5% HCl overnight before rinsing and drying down. Carbon isotope analysis was also  
202 carried out on palynology residues of the >250  $\mu\text{m}$  size fractions dominated by AOM.  $^{13}\text{C}/^{12}\text{C}$   
203 analyses were performed on 35 samples by combustion in a Costech Elemental Analyser (EA) on-  
204 line to a VG TripleTrap and Optima dual-inlet mass spectrometer, with  $\delta^{13}\text{C}$  values calculated to the  
205 VPDB scale using a within-run laboratory standards calibrated against NBS-18, NBS-19 and  
206 NBS-22. Replicate  $^{13}\text{C}/^{12}\text{C}$  analyses were carried out on the section, and the mean standard  
207 deviation on the replicate analyses is 0.4‰.

208

## 209 **4. Results and discussion**

210

### 211 *4.1. Statistical analysis*

212

213 Correspondence analysis (CA) and statistical diversity analysis was carried out on the  
214 palynological dataset (total counts per gram) to confirm assemblage designations (Figs. 4, 5), to  
215 identify any disturbance to the core prior to interpretation, and to estimate diversity (Fig. 6).  
216 Dinoflagellate cyst assemblages (DA1–DA5) and pollen assemblages (PA1–PA4) were defined by  
217 visually comparing changes in the species dominance (Figs. 7, 8), and confirmed by CA (Fig. 4)  
218 using the first three axes (describing the highest percentages of variance). Five samples from below  
219 the CIE at 2619.60, 2617.35, 2617.44, 2614.73 and 2614.71 m (indicated in Fig. 5) contain  
220 *Apectodinium*, in contrast to the other samples below the CIE (Figs 3, 7). Some of these samples  
221 (2619.60, 2614.73 and 2614.71 m) also contain negative  $\delta^{13}\text{C}_{\text{TOC}}$ , indicative of the CIE (Fig. 3). To  
222 test if coincident pollen and spore changes also occur in these samples, we used CA on the pollen  
223 and spore data only (Fig. 5a). PA1–PA4 (symbols) plot in clusters, signifying their palynological  
224 similarity. The species most associated with an assemblage are clustered with the samples from that  
225 assemblage. For example, *Inaperturopollenites hiatus* and bisaccate pollen (highly abundant before  
226 the CIE, Fig. 8) are high on axis 1 where the earlier samples from PA1 and PA2 occur, and  
227 *Caryapollenites* spp. and fungal spores (abundant after the CIE, Fig. 8) are low on axis 1 near the  
228 younger samples from PA4. The two samples 2619.60 and 2614.71 have a spore and pollen  
229 palynological signature similar to samples from PA3/4 during the CIE (plot lower on axis 1) and are  
230 either not in the correct location (it cannot be discounted that these samples were misplaced during  
231 drilling operations core handling), or represent very short episodes of both marine and terrestrial  
232 ecologic change to CIE-type conditions. The rapid and transient nature of these two shifts appears

233 to suggest that the latter explanation may be unlikely, and we have therefore shaded samples from  
234 these two depths in Figs. 3, 6, 7, 8, 9.

235 The majority of the morphospecies in our study represent taxonomic groupings of terrestrial  
236 plant species, from generic to higher level groupings, such that any palynology diversity measure  
237 will underestimate vegetation diversity. However, although subtle changes may not be resolved,  
238 large changes to the diversity of regional vegetation are likely to be reflected in palynology  
239 assemblages. Palynological data have therefore previously been used to estimate plant diversity in  
240 the geological record (e.g. Ogaard, 2001; Harrington, 2004; Jaramillo et al., 2010). The number of  
241 pollen and spore species in each sample (Fig. 6d) fluctuates, trending towards increasing number  
242 over the CIE onset (from PA2 to PA3). To account for the changing number of specimens counted  
243 in each sample (more species will be encountered with higher counts), two statistical indices were  
244 used (Fig. 6e, f). Both confirm the significant increase in pollen and spore diversity from before to  
245 after the CIE onset. We don't use the range-through method, as we are interested in changes to local  
246 vegetation habitats. The increase in the number of pollen and spore species appears to be largely  
247 driven by pteridophytes (largely ferns, Fig. 6g), although angiosperm diversity also increases over  
248 the CIE onset (Fig. 6h) and fungal spores become more prevalent (Fig. 8m). Gymnosperms are only  
249 represented by two morphospecies and so diversity was not calculated for this group.

250

#### 251 4.2. Isotope changes and age model

252

253 The Lista and Sele Formation boundary (Fig. 2) occurs in the lower part of magnetochron  
254 24r in the Faeroe-Shetland Basin (Mudge and Bujak, 2001), giving a date of  $>56.6$  Ma for the base  
255 of the studied section (Gradstein et al., 2004). The top of the studied section is within nannofossil  
256 zone NP9 (Knox, 1996), dated as  $<55.7$  Ma (Gradstein et al., 2004). The Paleocene-Eocene marker  
257 event *Apectodinium augustum* (Bujak and Brinkhuis 1998) occurs in 22/10a-4 at 2617.35 m (Fig.  
258 3), approximately at the CIE onset (as was found at 30/14-1, Fig. 1, Sluijs et al., 2007). The global  
259 CIE is determined by the negative shift in both marine and terrestrial  $\delta^{13}\text{C}$  of between  $\sim 2\text{‰}$  and  
260  $\sim 7\text{‰}$  (see Schouten et al., 2007) and has recently been radioisotopically dated in Spitsbergen to  
261  $\sim 55.8$  Ma (Charles et al., 2011). The global CIE onset is present in 22/10a-4 within the interval  
262  $\sim 2614$  to  $\sim 2612$  m (Fig. 3), where a negative  $\delta^{13}\text{C}$  shift of  $\sim 5\text{‰}$  occurs along with a peak in  
263 *Apectodinium*. The palynological results (from samples containing sufficient material for analysis;  
264 red symbols in Fig. 3) show that %wood/plant tissue varies from 10% to 88% throughout this  
265 interval (Fig. S3). We found that the samples containing  $>30\%$  wood/plant tissue (empty red  
266 symbols in Fig. 3) in the palynological residues have consistently heavier  $\delta^{13}\text{C}_{\text{TOC}}$  values than those  
267 with less wood/plant tissues (solid red symbols). The presence of transported  $\text{C}_{\text{org}}$  thus precludes an

268 unambiguous interpretation of the rate of atmospheric carbon release from the shape of the CIE  
269 onset at 22/10a-4, but the initial negative  $\delta^{13}\text{C}$  shift between 2614.3 and 2613.5 m (shaded box, Fig.  
270 3) can be taken as marking the earliest evidence of  $\delta^{13}\text{C}$ -depleted atmospheric carbon release and  
271 the onset of the global CIE. This positioning of the CIE onset is supported by  $\delta^{13}\text{C}$  analysis of  
272 isolated AOM (Fig. 3), likely of marine origin (see Supplementary Material) and less likely to be  
273 composed of mixtures of different sources of  $\text{C}_{\text{org}}$  (although it is still susceptible to reworking).

274 As we observe only a  $\sim 1\%$  ‘recovery’ in the CIE, the age of the top of the studied section  
275 appears to be no more than  $\sim 75$  ka from the CIE onset by comparison with the  
276 cyclostratigraphically correlated Longyearbyen Section in Spitsbergen (Charles et al., 2011), giving  
277 an average sedimentation rate of  $\geq 8$  cm/ka after the CIE onset (if sand horizons (Fig. 3) are  
278 removed, assuming rapid turbidite deposition). The long term  $\sim 0.7\%$  positive shift in  $\delta^{13}\text{C}$  at 2609  
279 m (Fig. 3) may correlate to a similar shift in the Longyearbyen Section (Charles et al., 2011), which  
280 is cyclostratigraphically correlated to  $\sim 45$  ka after the CIE onset (Charles et al., 2011), and would  
281 give a sedimentation rate of on average  $\sim 8$  cm/ka for this section. The finely laminated part of the  
282 core may also provide temporal insight. There is no direct evidence for the period of deposition of  
283 each lamination couplet, but as modern marine lamination-forming basins produce annual laminae  
284 pairs (e.g. the Black Sea: Arthur, 1994; Cariaco Basin: Tadesco and Thunell, 2003; Santa Barbara  
285 Basin: Thunell et al., 1995), the  $\sim 40,000$  estimate of the number of laminae pairs present between  
286  $\sim 2613$  and  $\sim 2609$  m (see Section 3.1) may represent  $\sim 40$  ka, and a sedimentation rate of  $\sim 7.5$   
287 cm/ka.

288

#### 289 4.3. *Dinoflagellate cysts and surface water changes*

290

291 Dinoflagellate cysts have been used extensively for reconstructing paleoenvironments in the  
292 Paleogene (see overview in Sluijs et al., 2005), as they are particularly sensitive to changes in  
293 salinity, temperature and nutrient levels (Powell et al., 1992; Pross and Brinkhuis 2005; Sluijs et al.,  
294 2005). We calculate “%low salinity dinoflagellate cysts” (Figs. 7–9) by grouping cysts of similar  
295 inferred ecologic preferences (see Fig. 7, and discussion in the Supplementary Material) to provide  
296 an indication of environmental change, and by excluding species of uncertain affinity such as  
297 *Apectodinium*. Samples with fewer than 20 specimens were also excluded. Despite the limitations  
298 of this method, the large variation in the %low salinity dinoflagellate cysts (ranging from 0–80%)  
299 clearly indicates that significant environmental changes in surface water conditions occurred during  
300 the CIE onset in the central North Sea, and is supported by coeval changes in the sedimentary  
301 carbon/nitrogen (C/N) ratio (Fig. 10) which reflects changes in the proportion of terrestrial/marine

302 organic material deposited in the North Sea Basin due to terrestrial runoff and productivity (see  
303 Section 4.4).

304 Dinoflagellate cyst assemblage 1 (DA1, ~2632 to 2618 m, Fig. 7p) contains high  
305 proportions of typically open marine and hence normal marine salinity associated  
306 *Achomosphaera/Spiniferites* spp., undifferentiated chorate cysts and *Areoligera/Glaphyrocysta* spp.  
307 DA1 also contains on average ~5% peridinoid cysts including *Deflandrea* spp. regarded as a  
308 coastal/neritic taxon indicating high productivity and nutrient availability (Brinkhuis, 1994; Pross  
309 and Brinkhuis, 2005). These characteristics indicate that a somewhat restricted but fully marine  
310 shelf environment was present before the onset of the CIE in the central North Sea, with availability  
311 of nutrients indicated by the presence of *Deflandrea* spp.

312 DA2 (~2618 to 2614 m) contains a similar abundance of *Achomosphaera/Spiniferites* spp.  
313 and chorate cysts to DA1, but with a marked increase in the abundance of low salinity tolerate  
314 *Cerodinium depressum* and *Senegalinium* spp., which may also have been a heterotrophic genus  
315 indicative of elevated nutrient levels (Sluijs and Brinkhuis, 2009). Undifferentiated peridinoid cysts  
316 also peak in abundance, and may also be indicative of elevated nutrient and reduced salinity  
317 conditions (although they are not included in the %low salinity dinoflagellate cysts, Fig. 7c). There  
318 is also an increase in the abundance of *Areoligera/Glaphyrocysta* spp., thought to indicate  
319 unrestricted neritic environments of more typical marine salinity. In summary, the higher proportion  
320 of low salinity tolerant dinoflagellate cysts in DA2 (Fig. 7c) appears to indicate continuous or  
321 episodic freshening surface waters below typical marine salinities (< ~31‰ in the modern ocean).  
322 In addition, DA2 is characterised by elevated numbers of dinoflagellate cysts per gram (~70 per  
323 0.05g in DA1, ~110 per 0.05g in DA2) indicating a possible increase in cyst production which  
324 would be consistent with increased fluvial runoff carrying nutrients from nearby landmasses. DA2  
325 also contains an abundance maxima of *Apectodinium*, an extinct genus with a somewhat uncertain  
326 ecologic affinity (see Crouch et al., 2003b), although likely reflecting relatively warm and eutrophic  
327 conditions (Crouch et al., 2003b; Sluijs et al., 2007; see Supplementary Material). The transient  
328 appearance of *Apectodinium* occurs with a reduced abundance of open marine dinoflagellates, and a  
329 peak in *Deflandrea* indicating possibly lower salinity and higher nutrient availability.

330 DA3 (~2614 to 2612 m) is characterised by *Apectodinium* making up on average ~40% of  
331 the assemblage, and a reduction in the abundance of all other species apart from *Deflandrea* and  
332 *Senegalinium*. DA3 may therefore indicate a continuation of high nutrient surface water with an  
333 elevated freshwater input. In this respect, it is perhaps similar to DA2, although the low abundances  
334 of dinoflagellates with known ecologic affinities make interpretations more tentative. The  
335 appearance of bottom water anoxia (laminations) and sporadic high accumulation of marine AOM  
336 (see Supplementary Material) is consistent with highly productive surface waters.

337 DA4 (~2612 to 2609 m) shows an increase in the number of low salinity/high nutrient  
338 species *Cerodinium depressum* and *Senegalinium* spp., with a continued low abundance of normal  
339 marine salinity *Achomosphaera/Spiniferites* spp., such that the proportion of low salinity tolerant  
340 dinoflagellate cysts is at a maximum (Fig. 7c) indicating the presence of a pronounced halocline.  
341 The lack of freshwater fern and algal spores *Azolla*, *Pediastrum* and *Botryococcus* (Table S1)  
342 indicates that surface water salinities were probably not below ~5‰ (the limit for *Azolla*, Brinkhuis  
343 et al., 2006), and may have been greater than ~20‰ as *Botryococcus* was found living in salinities  
344 as high as 20‰ in modern Australian lakes (de Deckker, 1988). This minimum salinity value is  
345 consistent with Zacke et al. (2009), who found continuous occurrences of shark teeth in shallow  
346 marine North Sea facies throughout the late Paleocene/early Eocene, and noted that sharks do not  
347 live in salinities below ~20‰ in the modern ocean. Highly productive surface waters are indicated  
348 by dinoflagellate cysts (Fig. 7c), and consistent with bottom water anoxia (laminations and  
349 disappearance of benthic foraminifera) and very high accumulation of marine AOM.

350 DA5 (~2609 to 2607 m) shows a decrease in low salinity tolerant dinoflagellate cysts and an  
351 increase in unrestricted (normal marine salinity) *Areoligera/Glaphyrocysta* spp. and other chorate  
352 cysts. The reduction in AOM together with the loss of lamination (possibly end of bottom water  
353 anoxia) indicates a return towards marine salinities that existed before the onset of the CIE  
354 (represented by DA1), although the persistence of *Apectodinium* may indicate a long term change in  
355 marine ecology.

356

#### 357 4.4. Enhanced terrigenous deposition

358

359 The increase in abundance of low salinity tolerant *Cerodinium depressum* and *Senegalinium*  
360 spp. before and after the CIE onset (DA2 to DA4, Fig. 7) most likely indicates a reduction in  
361 surface water salinity and elevated nutrient levels (see Section 4.3). This appears to have been  
362 associated with increased terrigenous deposition, as evidenced by a concomitant increase in the C/N  
363 ratio of 22/10a-4 (Figs. 9c, S4), and an elevated kaolinite contribution to the clay assemblage (Fig.  
364 9e). Sedimentary atomic C/N ratios can be used to differentiate the origin of organic matter  
365 (Meyers, 1997; Storme et al., 2012), with values in 22/10a-4 averaging ~10–15 (Fig. 10) indicating  
366 a mix of terrestrial land plant-derived and marine/lacustrine algal-derived carbon (Meyers, 1997).  
367 C/N values broadly follow %low salinity dinoflagellate cysts (Fig. 9), with an increase at the  
368 Lista/Sele Formation boundary, ~4 m before the onset of the CIE, and within the early CIE. As  
369 dinoflagellate cyst assemblages suggest higher productivity (%low salinity dinoflagellate cysts,  
370 *Apectodinium*), the C/N ratio increase likely indicates an increased flux of terrigenous material to  
371 22/10a-4, rather than a lower marine carbon flux. Kaolinite also increases before and after the onset

372 of the CIE in 22/10a-4 (Fig. 9e). Kaolinite forms as a result of intense chemical weathering that  
373 typically develops on well-drained surfaces receiving high precipitation (Robert and Kennett,  
374 1994). Increased kaolinite at the PETM had been regarded as indicative of an increase in chemical  
375 weathering and hence humidity in the source region (e.g. Robert and Kennett, 1994; Knox, 1996),  
376 but the long formation time of thick soil kaolinite (>1 myr) suggests these increased proportions  
377 probably resulted from erosion of previously-formed kaolinite (Thiry and Dupuis, 2000; Schmitz et  
378 al., 2001).

379

#### 380 4.5. Pollen, spores and vegetation shifts

381

382 The pollen and spore assemblages (PA) that characterise the pre-CIE interval in 22/10a-4  
383 (PA1 and PA2, Fig. 8n) are dominated by *I. hiatus* and bisaccate pollen. Both taxa are produced in  
384 abundance by a variety of coniferous plants, and are typical in the Paleogene of the northern UK  
385 and Greenland region (Boulter and Manum 1989; Jolley and Whitham 2004; Jolley and Morton  
386 2007), as well as mid-latitude North America (Smith et al., 2007) and Arctic Canada (Greenwood  
387 and Basinger, 1993). *I. hiatus* is a member of the Cupressaceae family (coniferous trees) and most  
388 likely represents *Metasequoia* and/or *Glyptostrobus* swamp conifers (Greenwood and Basinger,  
389 1993; Jolley and Morton, 2007; Jolley et al., 2009). In terrestrial Paleocene deposits from western  
390 Scotland, abundant *I. hiatus* was recorded in association with *Momipites*, *Cupuliferoipollenites*,  
391 *Platycaryapollenites*, *Plicapollis pseudoexcelsus*, and *Alnipollenites* interpreted as derived from a  
392 channel-margin bog community on a wet substrate (Jolley et al., 2009). Bisaccate pollen (family  
393 Pinaceae) was likely derived from temperate coniferous trees possibly on dryer substrates, with an  
394 elevation from several meters within swamps (Greenwood and Basinger, 1993) to possibly much  
395 higher altitude (Jolley and Whitham 2004). Both are relative overproducers of pollen (Smith et al.,  
396 2007). Lowland swamp vegetation appears to have been present before the CIE on the Scotland-  
397 Faeroe-Shetland platform (this study; Jolley and Morton 2007), the catchment area for 22/10a-4  
398 (Fig. S1, Knox 1996), with the relative increase of *I. hiatus* over bisaccate pollen from PA1 to PA2  
399 possibly due to sea level fall at the Lista/Sele boundary (Knox, 1996) allowing lowland swamp  
400 conifers to expand and/or come into closer proximity to 22/10a-4.

401 The most significant floral change at 22/10a-4 occurs at the onset of the CIE (PA2 to PA3),  
402 with a large drop in the proportion of *I. hiatus*, increasing diversity (Fig. 6), higher proportions of  
403 angiosperms (*Alnipollenites* and *P. pseudoexcelsus*), and fern and fungal spores (Fig. 8).  
404 *Alnipollenites* was probably from the birch *Alnus* (alder), and in this setting represents generalist  
405 vegetation as it occurred in all the terrestrial Paleocene communities from western Scotland (Jolley  
406 et al., 2009). *Alnus* and associated ferns were most common where *Metasequoia* (possible source of

407 *I. hiatus*) was rare in Arctic Canada, where exceptionally well-preserved Paleocene-Eocene  
408 *Metasequoia* and *Glyptostrobus* swamp deposits are prevalent, and interpreted as *Alnus*–fern bogs  
409 (Greenwood and Basinger, 1993). *Alnus* is a known nitrogen-fixing pioneer species in nutrient-  
410 depleted soils (Hobbie et al., 1998). *P. pseudoexcelsus* is similar to modern *Juglans* (walnut) pollen  
411 sometimes associated with wetland plants (Jolley and Whitham, 2004). The fern spores  
412 *Cicatricosisporites* and *Laevigatosporites* (family Schizaeaceae) were generalists, associated with  
413 all environments from the terrestrial Paleocene communities analysed in western Scotland (Jolley et  
414 al., 2009). Since dinoflagellate cysts indicate increased halocline stratification of the North Sea at  
415 the CIE (Fig. 9d), and C/N ratios indicate a greater proportion of terrestrial carbon (Fig. 9c), it  
416 seems likely that the large reduction in *I. hiatus* in 22/10a-4 reflects a change in vegetation cover in  
417 the source region rather than simply a general reduction in the supply of pollen due to proximity of  
418 the coast.

419 Replacement of *I. hiatus*-dominated swamp communities (PA2) with generalist taxa (PA3)  
420 indicative of *Alnus*–fern bogs (Greenwood and Basinger, 1993) would be consistent with local sea  
421 level fall (partially draining coastal plains) or sea level rise (flooding established coastal swamp  
422 plains). There is evidence for sea level rise at the onset of the CIE in southeast England (Powell et  
423 al., 1996) and in Spitsbergen (Harding et al., 2011), although any uplift associated with the  
424 proximal NAIP could have caused local sea level fall near the Faeroe-Shetland platform.  
425 Alternatively, the reduction in gymnosperm swamp conifers and pines at the expense of  
426 angiosperms may have been a climatic response to the PETM, as a similar floristic change was also  
427 recorded during the PETM in the Bighorn Basin, Wyoming (Smith et al., 2007), and the  
428 Lomonosov Ridge (Sluijs et al., 2006). The early ephemeral peak in *Alnipollenites* and *P.*  
429 *pseudoexcelsus* and drop in coastal swamp *I. hiatus* at 2617.35 m, associated with the initial peak in  
430 *Apectodinium* (Fig. 8), may indicate a brief episode of coastal flooding from increased precipitation,  
431 in association with lower surface water salinity (peak in *Deflandrea*, Fig. 7i).

432 A further ecologic shift occurs within the core of the CIE (PA4) as *Caryapollenites* (Fig. 8h)  
433 begins to dominate, moss (*Stereisporites*) and fungal spores increase in relative abundance,  
434 bisaccate pollen and *Alnipollenites* decreases (Fig. 8), and diversity remains relatively high (Fig. 6).  
435 *Caryapollenites*, similar to modern *Carya* (hickory) pollen, is common in terrestrial Paleocene  
436 deposits from western Scotland interpreted as bogs (Jolley et al., 2009), and many may have been  
437 adapted as primary colonisers in wet substrates (Jolley and Whitham 1994). Its association with  
438 moss and fern spores in PA4 indicates a possible predominance of bog environments, consistent  
439 with high regional precipitation and poorly drained acidic bedrock. As bogs receive water and  
440 nutrients directly from precipitation (Price and Waddington, 2000), the change from PA3 to PA4  
441 appears to be the result of climatic change (e.g. precipitation and temperature) rather than sea level.

442 Other changes include a further increase in the proportion of angiosperm over gymnosperm pollen  
443 (largely a reduction in pine), consistent with previous observations from the Lomonosov Ridge  
444 (Sluijs et al., 2006) and Bighorn Basin, Wyoming (Smith et al., 2007).

445

#### 446 *4.6. Environmental and climatic changes before the CIE*

447

448 The North Sea Basin became restricted before the PETM, as indicated by a lithologic  
449 change throughout the North Sea Basin (the Lista/Sele boundary, Figs. 2, 9) and the presence of low  
450 oxygen benthic foraminifera in 22/10a-4 (Knox, 1996). This relative sea level fall was recognised as  
451 a lithologic change from marine to lagoonal/shallow marine facies in southeast England (Knox et  
452 al., 1994) and considered to have been largely the result of major regional uplift possibly by ~100 m  
453 (Knox, 1996). The documented major tectonic uplift at the Lista/Sele boundary best explains the  
454 concomitant increase in terrigenous input to 22/10a-4 (increase C/N ratio, Fig. 9c), domination of  
455 lowland swamp vegetation (swamp conifers, Fig. 8), and the lowering of surface water salinity  
456 (dinoflagellate cysts, Fig. 9d) as the basin became more restricted. The gradual lowering of surface  
457 water salinity and increase in the C/N ratio from ~4 m before the CIE onset at 22/10a-4 (above  
458 ~2618 m, Fig. 9), therefore, may also be the result of further uplift and restriction of the North Sea  
459 Basin, bringing the coastline and transported terrestrial material into closer proximity to the  
460 centrally-located 22/10a-4, although there is no documented sea level fall in the North Sea  
461 preceding the CIE (Knox, 1996; Powell et al., 1996). The increase in kaolinite in this scenario  
462 would be coincidental, perhaps having been formed after (>1 myr, Thiry and Dupuis, 2000) the  
463 uplift at the List/Sele boundary. As the North Sea Basin was proximal to the NAIP during the  
464 Paleocene/Eocene (Figs. 1, S1), regional uplift before the CIE would most likely be related to  
465 intrusive activity west of the North Sea Basin, restricting deep-water connections between the North  
466 Sea and Atlantic Ocean. Uplift and restriction is therefore consistent with the hypothesis that a  
467 mantle-derived magmatic intrusion of organic-rich sediments occurred in the NE Atlantic before the  
468 CIE, triggering atmospheric methane release (Svensen et al., 2004).

469 Alternatively, an increase in regional precipitation could have caused elevated terrestrial  
470 runoff (C/N ratios, kaolinite) and lower surface water salinity above ~2618 m before the CIE onset  
471 (Fig. 9). The North Sea Basin surrounding landmasses were within the northern rain belt (the  
472 southern boundary today is ~40°N), which would have experienced elevated precipitation if the  
473 global hydrologic cycle became enhanced (Pagani et al., 2006b; Schmitz et al., 2001). This scenario  
474 would be consistent with a gradual increase in the global hydrologic cycle before the CIE, perhaps  
475 from gradual warming, which was hypothesised to have triggered ocean circulation changes,  
476 methane hydrate destabilisation, and global carbon release at the CIE (Bice and Marotzke, 2002).

477 We note however that there is currently no evidence for an enhanced hydrologic cycle well-before  
478 the CIE in other regions.

479 Our results provide the first evidence that the North Sea became stratified from ~4 m before  
480 the CIE onset (above ~2618 m, Fig. 9). This is significant as Nisbet et al. (2009) hypothesised that  
481 the proximal Kilda Basin become stratified and anoxic at before the CIE, allowing significant build-  
482 up of methane and CO<sub>2</sub> at depth. They proposed that overturning of this basin could have released  
483 greenhouse gases and triggered the CIE, although there is currently no direct evidence as marine  
484 records from the Kilda Basin remain rare (Nisbet et al., 2009). Our North Sea records likely indicate  
485 enhanced stratification also of the proximal and linked Kilda Basin before the CIE (Fig. 1).  
486 Evidence for the linkage of the North Sea, Kilda and Arctic Basins comes from the coincident onset  
487 of *A. augustum* and laminated sediments at the CIE onset in sections from the North Sea (this  
488 study), Spitsbergen (Harding et al., 2011) and Lomonosov Ridge (Sluijs et al., 2006). Although our  
489 results evidence a probable stratified Kilda Basin before the CIE, proxies for overturning are now  
490 needed to further test the Kilda basin hypothesis.

491 The brief peak in *Apectodinium*, AOM and low salinity dinoflagellate cysts (*Deflandrea*) at  
492 ~2617.4 m (Fig. 7) indicates a sporadic episode of surface water freshening/eutrophication before  
493 the CIE, which is best explained by an increase in regional precipitation due to its rapid nature. A  
494 coincident reduction in *I. hiatus* swamp conifers indicates possible disturbance of nearby coastal  
495 environments possibly from flooding (see Section 4.5). An associated reduction in  $\delta^{13}\text{C}$  may have  
496 been caused by stratification of the North Sea from an enhanced halocline, trapping <sup>12</sup>C-enriched  
497 organic carbon at depth. This scenario may also explain the other peaks in *Apectodinium* at 2619.6  
498 and 2614.7 m (although see Section 4.1).

499

#### 500 4.7. Environmental and climatic changes within the CIE

501

502 The influx of *Apectodinium* (indicating the onset of the CIE) at the Paleocene-Eocene  
503 boundary in southeast England occurred in characteristically marine assemblages following non-  
504 marine deposition, and was interpreted as an indication of relative sea level rise associated with a  
505 transgression immediately preceding a maximum flooding surface within the early PETM (Powell  
506 et al., 1996). Sea level rise at the CIE onset was also recorded in Arctic Spitsbergen (Harding et al.,  
507 2011). The large reduction lowland swamp pollen at the CIE onset of 22/10a-4 indicates a possible  
508 change in regional sea level. As there is no direct evidence for regional uplift causing further  
509 restriction of the North Sea Basin associated with the CIE onset, increased regional precipitation  
510 may have been the major cause of increased C/N ratios (elevated fluvial runoff) and dinoflagellate  
511 cyst changes (lower surface water salinity) at and following the CIE onset in 22/10a-4 (Fig. 9).

512 Although our records cannot distinguish changes to seasonality, which may have increased in the  
513 Pyrenees (Schmitz et al., 2001; Schmitz and Pujalte, 2007) and mid-latitude North America (Wing  
514 et al., 2005; Kraus & Riggins 2007), they are consistent with an overall increase in precipitation  
515 over NW Europe associated with the CIE. Our records therefore provide evidence consistent with  
516 the hypothesis that a northward migration of storm tracks occurred from an intensified hydrologic  
517 cycle as a result of global warming at the PETM, proposed by Pagani et al. (2006b) to explain  
518 elevated Arctic runoff during the PETM. As Pagani et al. (2006b) could not fully resolve the CIE  
519 onset due to incomplete core recovery, our records provide evidence that an enhanced hydrologic  
520 cycle may have occurred in approximate concert with global carbon release at the CIE onset.  
521 Alternatively, uplift of the NAIP could have caused further restriction and stratification of the North  
522 Sea. The reduction in %low salinity dinoflagellate cysts and the C/N ratio above ~2609 m (Fig. 9)  
523 may indicate a reduction in precipitation over NW Europe, or more likely tectonic subsidence  
524 causing the basin to become less restricted.

525

## 526 **5. Conclusions**

527

528 A negative carbon isotope excursion of ~5‰ has been identified from  $\delta^{13}\text{C}_{\text{TOC}}$  and  $\delta^{13}\text{C}_{\text{AOM}}$   
529 in an expanded Paleocene-Eocene boundary section from the central North Sea Basin.  
530 Palynological (dinoflagellate cyst, pollen and spore assemblages) and sedimentologic (C/N ratios  
531 and kaolinite) evidence indicates major changes occurred to marine and terrestrial environments in  
532 NW Europe both preceding and over the CIE. Enhanced halocline stratification and terrigenous  
533 input from ~4 m before the CIE may indicate tectonic uplift, supporting hypotheses for NAIP  
534 volcanism as a trigger for the CIE (Svensen et al., 2004), and/or increased terrigenous runoff and  
535 regional precipitation, supporting hypotheses of an enhanced hydrologic cycle triggering carbon  
536 release (Bice and Marotzke, 2002). A peak in *Apectodinium* before the CIE is interpreted as an  
537 ephemeral increase in terrestrial runoff causing local eutrophication. Further enhanced halocline  
538 stratification and terrigenous input at and immediately after the CIE onset, coupled with evidence  
539 for sea level rise in coastal areas, indicates possible increased regional precipitation over NW  
540 Europe. At this location (paleolatitude ~54°N) increased precipitation lends evidence to the  
541 hypothesis that a poleward migration of storm tracks from an enhanced hydrologic cycle resulted  
542 from global warming during the PETM (Pagani et al., 2006b).

543 Palynological spore and pollen assemblages from 22/10a-4 record a rapid major shift in  
544 vegetation at the CIE onset, with dominant swamp conifer communities and pines largely replaced  
545 by generalist taxa including fern and fungal spores and various angiosperms. A change to a  
546 dominance of angiosperm over gymnosperm pollen at the CIE onset has previously been recorded

547 in the Arctic (Sluijs et al., 2006) and Wyoming (Smith et al., 2007). The rapid reduction in lowland  
548 gymnosperm swamp pollen at the CIE onset may indicate a change in lowland topography from sea  
549 level alteration, and/or it may indicate ecologic changes driven by climate (e.g. precipitation and  
550 temperature). This floral shift occurs simultaneously with the first persistent appearance of  
551 *Apectodinium* in 22/10a-4, indicating that precursor CIE ecologic changes identified in NW Atlantic  
552 and North Sea marine records (Sluijs et al., 2007) had a terrestrial counterpart in the North Sea  
553 region. Longer term vegetation changes after the CIE onset indicate a move towards more diverse  
554 generalist angiosperm and pteridophyte communities (dominance of *Caryapollenites*, fern and  
555 fungal spores). The pollen and spore assemblages therefore indicate that long term ecologic change  
556 occurred in NW Europe probably in response to temperature and hydrologic changes during the  
557 PETM, but that the most dramatic changes recorded in 22/10a-4 occurred abruptly at the onset of  
558 the CIE.

559         Supplementary materials related to this article can be found online at doi: xxx

560

## 561 **Acknowledgements**

562

563         We thank Matthew Wakefield and BG Group for making core material available for  
564 analysis. We gratefully acknowledge two anonymous reviewers for enhancing the manuscript, and  
565 Appy Sluijs for constructively reviewing a previous version of the manuscript. The work is  
566 published with the approval of the Executive Director of the British Geological Survey (NERC).

567

## 568 **References**

569

- 570 Arthur, M.A., Dean, W.E., Neff, E.D., Hay, B.J., King, J., Jones, G., 1994. Varve calibrated records  
571 of carbonate and organic carbon accumulation over the last 2000 years in the Black Sea. *Global*  
572 *Biogeochem. Cy.* 8, 195–217.
- 573 Bains, S., Norris, R.D., Corfield, R.M., Faul, K.L., 2000. Termination of global warmth at the  
574 Palaeocene/Eocene boundary through productivity feedback. *Nature* 407, 171–174.
- 575 Bice, K.L., Marotzke, J., 2002. Could changing ocean circulation have destabilized methane hydrate  
576 at the Paleocene/Eocene boundary? *Paleoceanography* 17, 1018, doi: 10.1029/2001PA000678
- 577 Boulter, M.C., Manum, S.B., 1989. The Brito-Arctic igneous province flora around the  
578 Paleocene/Eocene boundary. In: Eldholm, O., Thiede, J., Taylor, E., et al., 1989. *Proceedings*  
579 *of the Ocean Drilling Program, Scientific Results*, vol. 104, 663–680.

580 Brinkhuis, H., Schouten, S., Collinson, M.E., Sluijs, A., Sinninghe Damsté, J.S., Dickens, G.R.,  
581 Huber, M., Cronin, T.M., Jonaotaro Onodera, J., Takahashi, K., Bujak, J.P., Stein, R., van der  
582 Burgh, J., Eldrett, J.S., Harding, I.C., Lotter, A.F., Sangiorgi, F., Cittert, H., de Leeuw, J.W.,  
583 Matthiessen, J., Backman, J., Moran, K., the Expedition 302 Scientists, 2006. Episodic fresh  
584 surface waters in the Eocene Arctic Ocean. *Nature* 441, 606–609.

585 Brinkhuis, H., 1994. Late Eocene to early Oligocene dinoflagellate cysts from the Priabonian tye  
586 area (northeast Italy); biostratigraphy and palaeoenvironmental interpretation. *Palaeogeogr.*  
587 *Palaeoclimatol. Palaeoecol.* 107, 121–163.

588 Bujak, J., Brinkhuis, H., 1998. Global Warming and Dinocyst Changes across the  
589 Palaeocene/Eocene Epoch Boundary. In: Aubry, M.-P., Lucas, S.G., Berggren, W.A. (Eds.),  
590 Late Palaeocene–Early Eocene Biotic and Climatic Events in Marine and Terrestrial Records.  
591 Columbia Univ. Press, New York, pp. 277–295.

592 Charles, A.J., Condon, D.J., Harding, I.C., Palike, H., Marshall, J.E.A., Cui, Y., Kump, L.,  
593 Croudace, I.W., 2011. Constraints on the numerical age of the Paleocene-Eocene boundary.  
594 *Geochem. Geophys. Geosyst.* 12, Q0AA17. doi: 10.1029/2010GC003426

595 Collinson, M.E., Steart, D.C., Scott, A.C., Glasspool, I.J., Hooker, J.J., 2007. Episodic fire, runoff  
596 and deposition at the Palaeocene-Eocene boundary. *J. Geol. Soc. Lond.* 164, 87–97.

597 Collinson, M., Steart, C.C., Harrington, G.J., Hooker, J.J., Scott, A.C., Allen, L.O., Glasspool, I.J.,  
598 Gibbons, S.J., 2009. Palynological evidence of vegetation dynamics in response to  
599 palaeoenvironmental change across the onset of the Paleocene-Eocene Thermal Maximum at  
600 Cobham, Southern England. *Grana* 48, 38–66.

601 Crouch, E.M., Dickens, G.R., Brinkhuis, H., Aubry, M., Hollis, C.J., Rogers, K.M., Visscher, H.,  
602 2003a. The Apectodinium acme and terrestrial discharge during the Paleocene–Eocene  
603 Thermal Maximum: new palynological, geochemical and calcareous nannoplankton  
604 observations at Tawanui, New Zealand. *Palaeogeogr. Palaeoclimatol. Palaeoecol.* 194, 387–  
605 403.

606 Crouch, E.M., Brinkhuis, H., Visscher, H., Adatte, H., Bolle, M.–P., 2003b. Late Palaeocene–early  
607 Eocene Dinoflagellate Cyst Records from the Tethys; Further Observations on the Global  
608 Distribution of Apectodinium. In: Wing, S., Gingerich, P.D., Schmitz, B., Thomas, E. (Eds.),  
609 Causes and Consequences of Globally Warm Climates in the Early Paleogene: *Geol. Soc. Am.*  
610 *Spec. Pap.*, vol. 369. Geological Society of America Inc., Boulder, Colorado, pp. 113–131.

611 Cui, Y., Kump, L.R., Ridgwell, A.J., Charles, A., Junium, C.K., Diefendorf, A.F., Freeman, K.H.,  
612 Urban, N.M., Harding, I.C., 2011. Slow release of fossil carbon during the Palaeocene-Eocene  
613 Thermal Maximum. *Nature Geosci.* 4, 481–485.

614 Dickens, G.R., O'Neil, J.R., Rea, D.K., Owen, R.M., 1995. Dissociation of oceanic methane  
615 hydrate as a cause of the carbon isotope excursion at the end of the Paleocene.  
616 *Paleoceanography* 10, 965–971.

617 Gillmore, G.K., Kjennerud, T., Kyrkjebø, R. 2001. The reconstruction and analysis of palaeo-water  
618 depths: a new approach and test of micropalaeontological approaches in the post-rift  
619 (Cretaceous to Quaternary) interval of the Northern North Sea. In: Martinsen, O.J., Dreyer, T.  
620 (Eds.), *Sedimentary environments offshore Norway – Palaeozoic to Recent*. Norwegian  
621 Petroleum Society (NPF), Special Publication 10, pp. 365–382.

622 Gonzalez, P., Neilson, R.P., Lenihan, J.M., Drapek, R.J., 2010. Global patterns in the vulnerability  
623 of ecosystems to vegetation shifts due to climate change. *Global Ecol. Biogeogr.* 6, 755-768.

624 Gradstein, F.M., Kristiansen, I.L., Loemo, L., Kaminski, M.A., 1992. Cenozoic foraminiferal and  
625 dinoflagellate cyst biostratigraphy of the Central North Sea. *Micropaleontology* 38, 101-137.

626 Gradstein, F.M., Ogg, J.G., 2005. *A Geologic Time Scale 2004*. Cambridge University Press,  
627 Cambridge, pp. 589.

628 Greenwood, D.R., Basinger, J.F., 1993. Stratigraphy and floristics of Eocene swamp forests from  
629 the Axel Heiberg Island, Canadian Arctic Archipelago. *Can. J. Earth. Sci.* 30, 1914-1923.

630 Hammer, Ø, Harper, D., Ryan, P.D., 2005. PAST: Palaeontological statistics software package for  
631 education and data analysis. *Palaeontologia Electronica* 4, pp. 9.

632 Harding, I.C., Charles, A.J., Marshall, J.E.A., Pälike, H., Roberts, A.P., Wilson, P.A., Jarvis, E.,  
633 Thorne, R., Morris, E., Moremon, R., Pearce, R.B., Akbari, S., 2011. Sea-level and salinity  
634 fluctuations during the Paleocene-Eocene thermal maximum in Arctic Spitsbergen. *Earth  
635 Planet. Sci. Lett.* 303, 97-107.

636 Harrington, G.J., 2004. Structure of the North American vegetation gradient during the late  
637 Paleocene/early Eocene warm climate. *Evolutionary Ecology Research* 6, 33-48.

638 Hobbie, E.A., Macko, S.A., Shugart, H.H., 1998. Patterns in N dynamics and N isotopes during  
639 primary succession. *Chem. Geol.* 152, 3–11.

640 Jaramillo, C., Ochoa, D., Contreras, L., Pagani, M., Carvajal-Ortiz, H., Pratt, L.M., Krishnan, S.,  
641 Cardona, A., Romero, M., Quiroz, L., Rodriguez, G., Rueda, M.J., de la Parra, F., Moro´n, S.,  
642 Green, W., Bayona, G., Montes, C., Quintero, O., Ramirez, R., Mora, G., Schouten, S.,  
643 Bermudez, H., Navarrete, R., Parra, F., Alvará n, M., Osorno, J., Crowley, J.L., Valencia, V.  
644 and Vervoort, J., 2010. Effects of rapid global warming at the Paleocene-Eocene boundary on  
645 neotropical vegetation. *Science* 330, 957–961.

646 Jolley, D.W., Morton, A.G., 2007. Understanding basin sedimentary provenance: evidence from  
647 allied phytogeographic and heavy mineral analysis of the Palaeocene of the NE Atlantic. *J.  
648 Geol. Soc. London* 164, 553-563.

649 Jolley, D.W., Bell, B.R., Williamson, I.T., Prince, I., 2009. Syn-eruption vegetation dynamics,  
650 paleosurfaces and structural controls on lava field vegetation: An example from the Palaeogene  
651 Staffa Formation. *Rev. Palaeobot. Palynol.* 153, 19-33.

652 Jolley, D.W., Whitham, A.G., 2004. A stratigraphical and palaeoenvironmental analysis of the sub-  
653 basaltic Palaeogene sediments of East Greenland. *Petroleum Geosci.* 10, 53-60 (2004).

654 Kennett, J.P., Stott, L.D., 1991. Abrupt deep-sea warming, palaeoceanographic changes and benthic  
655 extinctions at the end of the Palaeocene. *Nature* 353, 225–229.

656 Kjennerud, T., Gillmore, G.K., 2003. Integrated Palaeogene palaeobathymetry of the northern  
657 North Sea. *Pet. Geosci.* 9, 125–132.

658 Kjennerud, T., Sylta, Ø., 2001. Application of quantitative palaeobathymetry in basin modelling,  
659 with particular reference to the northern North Sea. *Pet. Geosci.* 7, 331–341.

660 Knox, R.W.O'B., 1996. Correlation of the early Paleogene in northwest Europe: an overview. In:  
661 Knox, R.W.O'B., Corfield, R., Dunay, R.E. (Eds.), *Correlation of the Early Paleogene in*  
662 *Northwest Europe. Special Publication, vol. 101. Geological Society of London, pp. 1-11.*

663 Knox, R.W.O'B., 1998. The tectonic and volcanic history of the North Atlantic region during the  
664 Paleocene-Eocene transition: implications for NW European and global biotic events. In:  
665 Aubry, M.-P., Lucas, S.G., Berggren, W.A. (Eds.), *Columbia Univ. Press, New York, pp. 91-*  
666 *102.*

667 Knox, R.W.O'B., Hine, N., Ali, J., 1994. New information on the age and sequence stratigraphy of  
668 the type Thanetian of Southeast England. *Newslet. Strat.* 30, 45–60.

669 Kraus, M.J., Riggins, S., 2007. Transient drying during the Paleocene-Eocene Thermal Maximum  
670 (PETM): analysis of paleosols in the Bighorn Basin, Wyoming. *Palaeogeogr. Palaeoclimatol.*  
671 *Palaeoecol.* 245, 444-461.

672 Lunt, D.J., Valdes, P.J., Dunkley Jones, T., Ridgwell, A., Haywood, A.M., Schmidt, D.N., Marsh,  
673 R., Maslin, M., 2010. CO<sub>2</sub>-driven ocean circulation changes as an amplifier of Paleocene-  
674 Eocene thermal maximum hydrate destabilisation. *Geology* 38, 875-878.

675 McInterney, F.A., Wing, S.L., 2011. The Paleocene-Eocene Thermal Maximum: A Perturbation of  
676 Carbon Cycle, Climate, and Biosphere with Implications for the Future. *Ann. Rev. Earth*  
677 *Planet. Sci.* 39, 489–516.

678 Meyers, P.A., 1997. Organic geochemical proxies of paleoceanographic, paleolimnologic, and  
679 paleoclimatic processes. *Org. Geoch.* 27, 213–250.

680 Moore, P.B., Webb, J.A., Collinson, M.E., 1991. *Pollen Analysis. Blackwell Scientific*  
681 *Publications, Oxford, Second Edition, pp. 216.*

682 Mosar, J., Torsvik, T.H., BAT team, 2002. Opening of the Norwegian and Greenland Seas: Plate  
683 Tectonics in Mid Norway since the Late Permian. In: Eide, E.A. (Ed.), *BATLAS – Mid*

684 Norway plate reconstructions atlas with global and Atlantic perspectives: Geol. Surv. Norway,  
685 pp. 48–59.

686 Mudge, D.C., Bujak, J.P., 2001. Biostratigraphic evidence for evolving palaeoenvironments in the  
687 Lower Paleogene of the Faeroe-Shetland Basin. *Marine and Petroleum Geology* 18, 577-590.

688 Nisbet, E.G., Jones, S.M., Maclennan, J., Eagles, G., Moed, J., Warwick, N., Bekki, S., Braesicke,  
689 P., Pyle, J.A., Fowler, C.M.R., 2009. Kick-starting ancient warming. *Nature Geosci.* 2, 156-  
690 159.

691 Ogaard, B.V., 2001. Palaeoecological perspectives on pattern and process in plant diversity and  
692 distribution adjustments: a comment on recent developments. *Diversity and Distributions* 4,  
693 197-201.

694 Pagani, M., Caldera, K., Archer, D., Zachos, J.C. 2006a. An ancient carbon mystery. *Nature* 314,  
695 1556-1557.

696 Pagani, M., Pedentchouk, N., Huber, M., Sluijs, A., Schouten, S., Brinkhuis, H., Sinninghe Damsté,  
697 J.S., Dickens, G.R., Expedition 302 Scientists, 2006b. Arctic hydrology during global warming  
698 at the Palaeocene/Eocene Thermal Maximum. *Nature* 442, 671–675.

699 Powell, A.J., Lewis, J., Dodge, J.D., 1992. A palynological expression of post-Palaeogene  
700 upwelling: a review. In: Prell, C.P., Emeis, K.C. (Eds.), *Upwelling systems: Evolution since the*  
701 *Early Miocene*. Special Publication, vol. 64. Geological Society of London, pp. 215-226.

702 Powell, A.J., Brinkhuis, H., Bujak, J.P., 1996. Upper Paleocene–lower Eocene Dinoflagellate Cyst  
703 Sequence Biostratigraphy of South-east England. In: Knox, R.W., Dunay, R.E., Corfield, R.M.  
704 (Eds.), *Correlation of the Early Paleogene in Northwest Europe: Special Publication*, vol. 101.  
705 Geological Society of London, pp. 145–183.

706 Price, J.S., Waddington, J.M. 2000. Advances in Canadian wetland hydrology and biogeography.  
707 *Hydrological Processes* 14, 1579-1589.

708 Pross, J., Brinkhuis, H., 2005. Organic-walled dinoflagellate cysts as paleoenvironmental indicators  
709 in the Paleogene; a synopsis of concepts. *Paläontologische Zeitschrift* 79, 53-59.

710 Röhl, U., Westerhold, T., Bralower, T.J., Zachos, J.C., 2007. On the duration of the Paleocene-  
711 Eocene thermal maximum (PETM). *Geochem. Geophys. Geosyst.* 8, Q12002,  
712 doi:10.1029/2007GC001784.

713 Robert, C., Kennett, J.P., 1994. Antarctic subtropical humid episode at the Paleocene-Eocene  
714 boundary: Clay-mineral evidence. *Geology* 22, 211-214.

715 Rull, V., 2011. A quantitative palynological record from the Early Miocene of western Venezuela,  
716 with emphasis on mangroves. *Palynology* 25, 109-126.

717 Schmitz, B., Pujalte, V., 2007. Abrupt increase in seasonal extreme precipitation at the Paleocene-  
718 Eocene boundary. *Geology* 35, 215-218.

719 Schmitz, B., Pujalte, V., Núñez-Betelu, K., 2001. Climate and sea-level perturbations during the  
720 Initial Eocene Thermal Maximum: evidence from siliciclastic units in the Basque Basin  
721 (Ermua, Zumaia and Trabakua Pass), northern Spain. *Palaeogeogr. Palaeoclimatol. Palaeoecol.*  
722 165, 299–320.

723 Schouten, S., Woltering, M., Rijpstra, I.C., Sluijs, A., Brinkhuis, H., Sinninghe Damsté, J.S., 2007.  
724 The Paleocene–Eocene carbon isotope excursion in higher plant organic matter: differential  
725 fractionation of angiosperms and conifers in the Arctic. *Earth Planet. Sci. Lett.* 258, 581–592.

726 Seager, R., Naik, N., Vecchi, G.A., 2010. Thermodynamic and dynamic mechanisms for large-scale  
727 changes in the hydrological cycle in response to global warming. *J. Climate* 23, 4651–4668.

728

729 Sluijs, A., Brinkhuis, H., 2009. A dynamic climate and ecosystem state during the Paleocene–  
730 Eocene Thermal Maximum: inferences from dinoflagellate cyst assemblages on the New Jersey  
731 Shelf. *Biogeosciences* 6, 1755–1781.

732 Sluijs, A., Pross, J., Brinkhuis, H., 2005. From greenhouse to icehouse; organic-walled  
733 dinoflagellate cysts as paleoenvironmental indicators in the Paleogene. *Earth Sci. Rev.* 68, 281–  
734 315.

735 Sluijs, A., Schouten, S., Pagani, M., Woltering, M., Brinkhuis, H., Sinninghe Damsté, J.S., Dickens,  
736 G.R., Huber, M., Reichert, G.J., Stein, R., Matthiessen, J., Lourens, L.J., Pedentchouk, N.,  
737 Backman, J., Moran, K., Expedition 302 Scientists, 2006. Subtropical Arctic Ocean  
738 temperatures during the Palaeocene–Eocene Thermal Maximum. *Nature* 441, 610–613.

739 Sluijs, A., Brinkhuis, H., Schouten, S., Bohaty, S.M., John, C.M., Zachos, J.C., Reichert, G.,  
740 Sinninghe Damsté, J.S., Crouch, E.M., Dickens, G.R., 2007. Environmental precursors to light  
741 carbon input at the Paleocene/Eocene boundary. *Nature* 450, 1218–1221.

742 Smith, F.A., Wing, S.L., Freeman, K.H., 2007. Magnitude of the carbon isotope excursion at the  
743 Paleocene-Eocene thermal maximum: The role of plant community change. *Earth Planet. Sci.*  
744 *Lett.* 258, 50–65.

745 Stephenson, M.H., Leng, M.J., Vane, C.H., Osterloff, P.L., Arrowsmith, C., 2005. Investigating the  
746 record of Permian climate change from argillaceous sediments, Oman. *J. Geol. Soc. London*  
747 162, 641–651.

748 Storme, J.-Y., Dupuis, C., Schnyder, J., Quesnel, F., Garel, S., Iakovleva, A.I., Iacumin, P., Matteo,  
749 A.D., Sebilo, M., Yans, J., 2012. Cycles of humid-dry climate conditions around the P/E  
750 boundary: new stable isotope data from terrestrial organic matter in Vasterival section (NW  
751 France). *Terra Nova* 24, 114–122.

752 Svensen H, Planke S, Malthe-Sorensen A, Jamtveit B, Myklebust R, Eidem, T.R., Rey, S.S., 2004.  
753 Release of methane from a volcanic basin as a mechanism for initial Eocene global warming.  
754 Nature 429, 542–545.

755 Tedesco, K.A., Thunell, R.C., 2003. Seasonal and interannual variations in planktonic foraminiferal  
756 flux and assemblage composition in the Cariaco Basin, Venezuela. *J. Foram. Res.* 33, 192-210.

757 Thiry, M, Dupuis, M., 2000. Use of clay minerals for paleoclimatic reconstructions: limits of the  
758 method with special reference to the Paleocene–lower Eocene interval. *GFF* 122, 166–67.

759 Thunell, R. C., Tappan, E., Anderson, D.M., 1995. Sediment fluxes and varve formation in Santa  
760 Barbara Basin, offshore California. *Geology* 23, 1083-1086.

761 Wing, S.L., Harrington, G.J., Smith, F.A., Bloch, J.I., Boyer, D.M., Freeman, K.H., 2005. Transient  
762 floral change and rapid global warming at the Paleocene–Eocene boundary. *Science* 310, 993–  
763 996.

764 Zachos, J.C., Röhl, U., Schellenberg, S.A., Sluijs, A., Hodell, D.A., Kelly, D.C., Thomas, E.,  
765 Nicolo, M., Raffi, I., Lourens, L.J., McCarren, H., Kroon, D., 2005. Rapid acidification of the  
766 ocean during the Palaeocene–Eocene thermal maximum. *Science* 308, 1611–1615.

767 Zacke, A., Voigt, S., Joachimski, M.M., Gale, A.S., Ward, D.J., Tütken, T., 2009. Surface-water  
768 freshening and high latitude river discharge in the Eocene of the North Sea. *J. Geol. Soc.*  
769 London 166, 969-980.

770 Zeebe, R.E., Zachos, J.C., Dickens, G.R., 2009. Carbon dioxide forcing alone insufficient to explain  
771 Palaeocene-Eocene Thermal Maximum warming. *Nature Geosci.* 2, 576-580.

772

773 **Display material captions:**

774

775 **Fig. 1.** Paleogeographic reconstruction of the continents at ~54 Ma (Mosar et al., 2002), showing  
776 the location of core 22/10a-4 (this study), 30/14-1 (Sluijs et al., 2007), 208/19-1 (Mudge and Bujak,  
777 2001), Spitsbergen Central Basin (Harding et al., 2011) and M0002A (Pagani et al., 2006b). Grey  
778 shading indicates regions of volcanism affected by the North Atlantic Igneous Province (NAIP).

779

780 **Fig. 2.** Lithologic column of borehole 22/10a-4 showing Gamma Ray Attenuation (GRA),  
781 stratigraphic and lithologic subdivisions, and previously published low resolution palynological and  
782 sedimentologic results (Knox, 1996). Depth is logging depth (all other depths in this paper are core  
783 depth). The GRA spike and onset of abundant *Apectodinium* was previously used to identify the  
784 position of the CIE (Knox, 1996). The extent of core analysed in this study is also shown. Yellow =  
785 sandstone; blue = massive grey claystone; light grey = intermittently bedded grey claystone; dark  
786 grey = well-bedded grey mudstone (Knox, 1996).

787

788 **Fig. 3.** Carbon isotopic results of total organic matter ( $\delta^{13}\text{C}_{\text{TOC}}$ ) and amorphous organic matter  
789 ( $\delta^{13}\text{C}_{\text{AOM}}$ ), against core 22/10a-4 lithology and *Apectodinium* spp. (%). Blue = bulk rock  $\delta^{13}\text{C}_{\text{TOC}}$ ;  
790 black =  $\delta^{13}\text{C}_{\text{AOM}}$ ; solid red symbols = bulk rock  $\delta^{13}\text{C}_{\text{TOC}}$  from samples with <30% wood/plant tissue  
791 (determined from palynological residue of the sample); open red symbols = bulk rock  $\delta^{13}\text{C}_{\text{TOC}}$  from  
792 samples with >30% wood/plant tissue. The first appearance of *Apectodinium augustum* identifies  
793 the PETM in the North Sea (Bujak and Brinkhuis, 1998), and the first negative shift in  $\delta^{13}\text{C}$   
794 identifies the approximate position of the CIE onset and the Paleocene-Eocene boundary. Values  
795 shaded at 2614.7 and 2619.6 m are considered possible outliers based on statistical analysis of the  
796 palynological residues (see Section 4.1). Lithologic column shows position of sand intervals  
797 (yellow), claystone intervals (brown; predominantly laminated claystone, dark brown), and ash  
798 layers (pink).

799

800 **Fig. 4.** Correspondence analysis for (a) dinoflagellate cysts, and (b) spores and pollen, from each  
801 sample (total counts per gram) in core 22/10a-4. First three axes are plotted against depth, with %  
802 variance indicated. Solid vertical lines indicate mean, dashed lines indicate standard deviation  
803 ( $\pm 1\sigma$ ). Values outside  $\pm 1\sigma$  are considered statistically meaningful and used to define pollen  
804 assemblages (PA) and dinoflagellate cyst assemblages (DA). The two circled values indicate  
805 samples that fall outside PA2, and either represent ephemeral episodes of vegetation changes to  
806 post-CIE onset type conditions, or possible misplaced samples during drilling operations core  
807 handling. Analysis carried out using the software of Hammer et al. (2005).

808

809 **Fig. 5.** Correspondence analysis (first two axes) for (a) spores and pollen species (total counts per  
810 gram, axis 1 = 39% of total variance, axis 2 = 17% of total variance), and (b) dinoflagellate cysts  
811 (total counts per gram, axis 1 = 31% of total variance, axis 2 = 11% of total variance), in core  
812 22/10a-4. Symbols indicate depths for each pollen assemblage (PA) and dinoflagellate cyst  
813 assemblage (DA), and their correspondingly most associated palynomorph species. Marked depths  
814 (red) indicate the samples with pre-CIE peaks in *Apectodinium* and  $\delta^{13}\text{C}_{\text{TOC}}$ . Samples at 2619.60 m  
815 and 2614.71 m (see Fig. 4) plot close to post-CIE onset assemblages PA3 and PA4, and either  
816 represent ephemeral episodes of marine and vegetation changes to post-CIE onset type conditions,  
817 or possible misplaced samples during drilling operations core handling. Analysis carried out using  
818 the software of Hammer et al. (2005).

819

820 **Fig. 6.** Spore and pollen abundance and diversity data from 22/10a-4. (a) Lithologic formations, (b)  
821 bulk total organic carbon (TOC) stable isotopes, (c) total abundance of all pollen/spores, (d) total  
822 number of pollen and spore species recorded in each sample, (e) diversity index Shannon H  
823 (calculated using the software of Hammer et al., 2005) which takes into account the number of  
824 specimens in each sample in addition to species, (f) diversity index Fisher alpha (calculated using  
825 the software of Hammer et al., 2005) which takes into account the number of specimens in each  
826 sample in addition to species, (g) total number of pteridophyte spore species recorded in each  
827 sample, (h) total number of angiosperm pollen species recorded in each sample.

828

829 **Fig. 7.** Sedimentologic, isotopic and micropaleontologic data for North Sea core 22/10a-4 (this  
830 study). Blue shaded area represents time of lowest surface water salinity (from dinoflagellate cysts)  
831 and inferred halocline stratification. (a) Lithologic formations, (b) bulk total organic carbon (TOC)  
832 isotopes, (c) dinoflagellate cysts tolerant of low salinity and high nutrients as percentage of all  
833 dinoflagellate cysts with known salinity preference, (d) benthic foraminifera (agglutinated), (e)  
834 amorphous organic matter (AOM) as a percentage of all palynomorphs, (f) position of finely  
835 laminated sediment, (g) % dinoflagellate cysts to spores and pollen, (h) *Apectodinium* spp. as  
836 percentage of all dinoflagellate cysts, (i-l) dinoflagellate cysts likely tolerant to low salinity and  
837 high nutrient surface water, (m-o) dinoflagellate cysts representative of typical marine salinity  
838 surface water, (p) dinoflagellate cyst assemblages (DA).

839

840 **Fig. 8.** Sedimentologic, isotopic and micropaleontologic data for North Sea core 22/10a-4 (this  
841 study). (a) Lithologic formations, (b) bulk total organic carbon (TOC) isotopes, (c) dinoflagellate  
842 cysts tolerant of low salinity and high nutrients as percentage of all dinoflagellate cysts with known

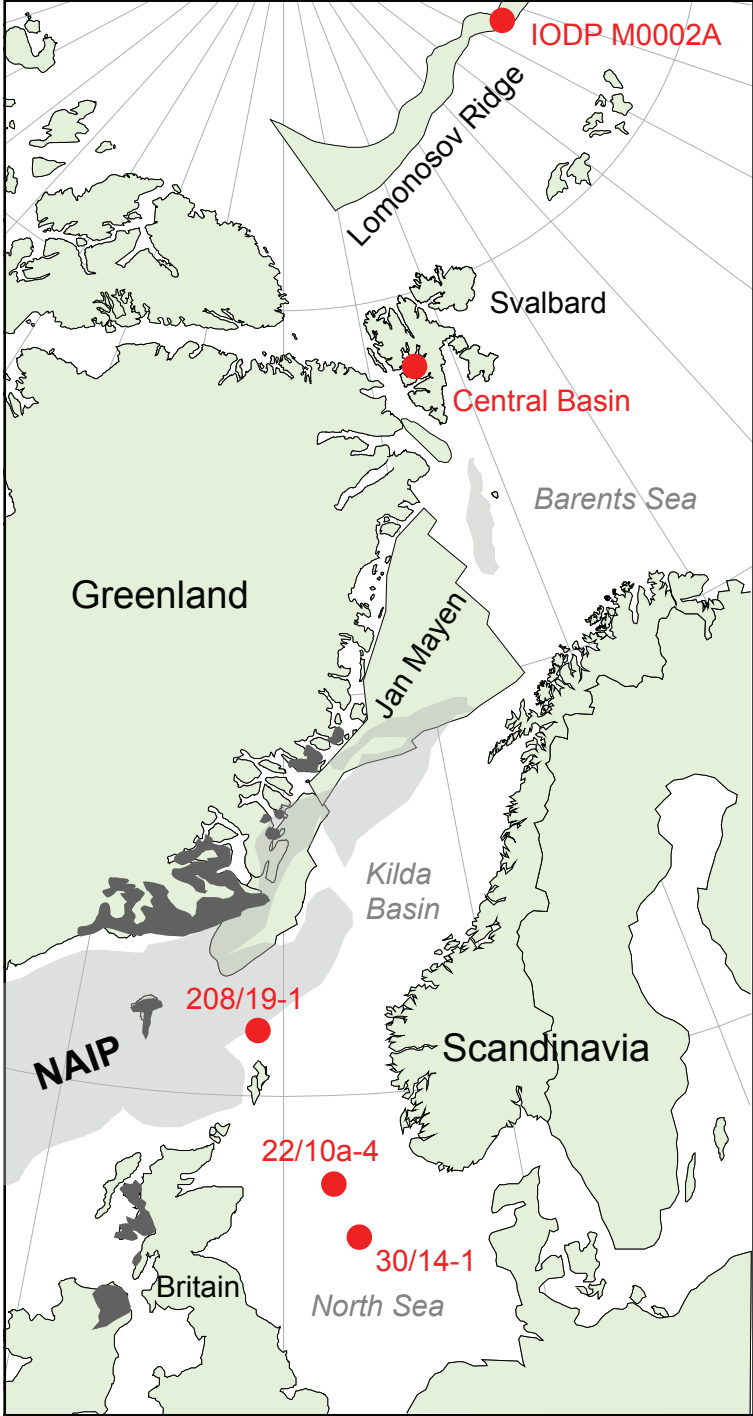
843 salinity preference, (d) angiosperm pollen as percentage of all angiosperm and gymnosperm pollen,  
844 (e) total abundance of all pollen/spores, (f-g) pre-CIE pollen, (h-l) pollen and spores prevalent in the  
845 CIE, (m) fungal spores, (n) pollen/spore assemblages (PA).

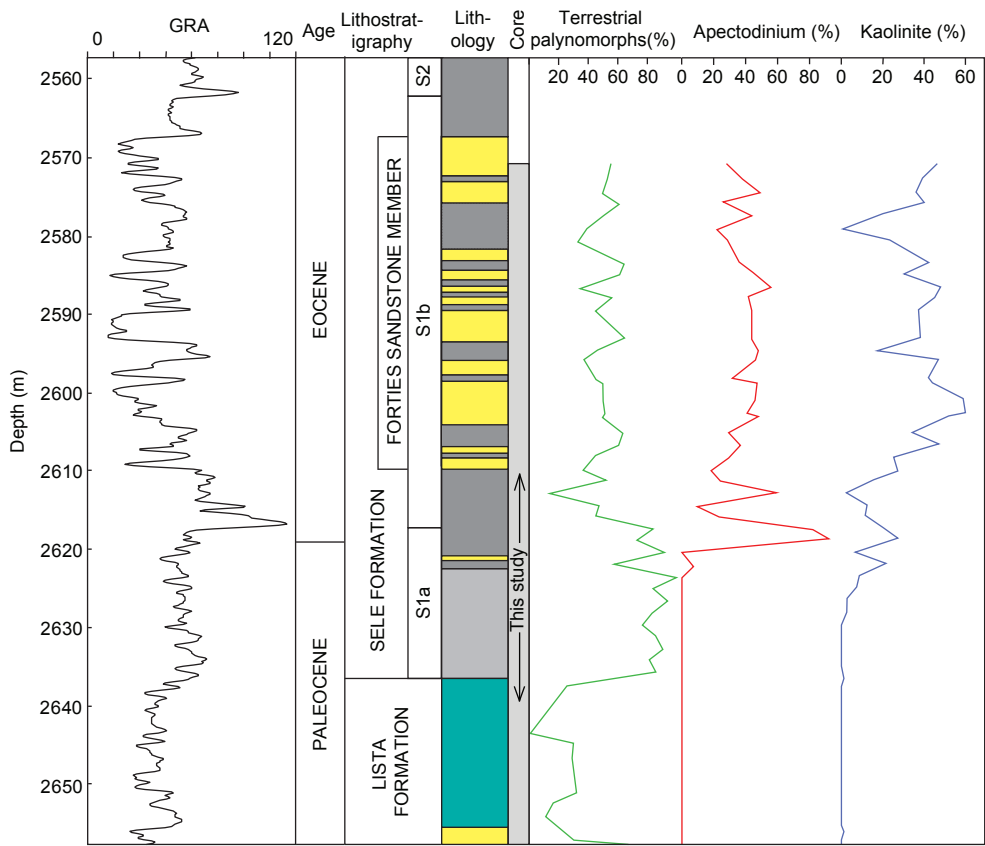
846

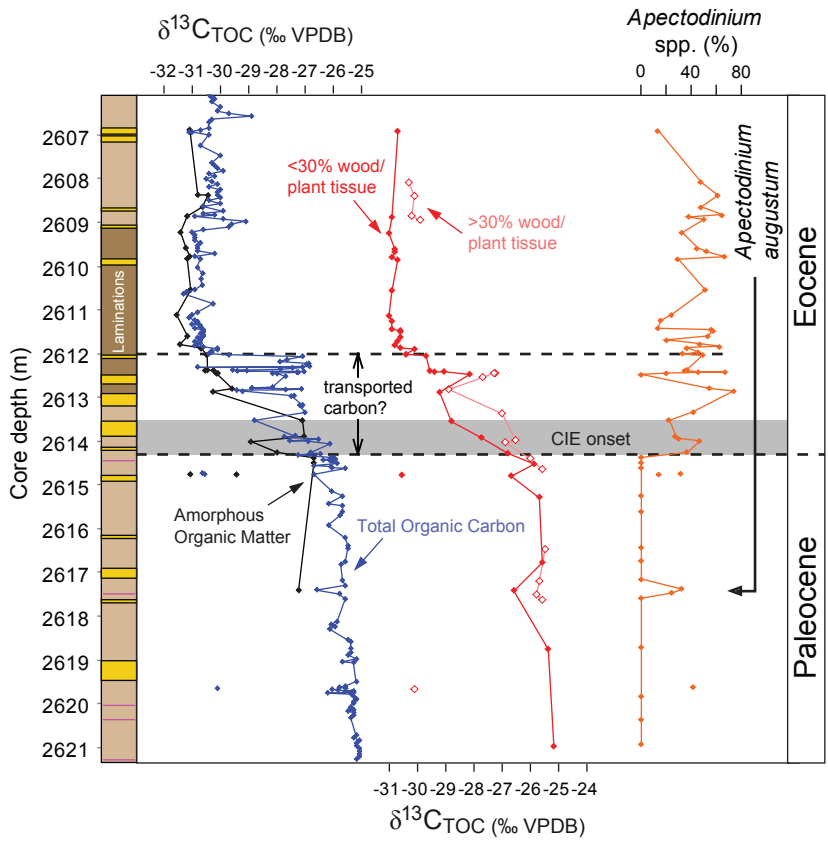
847 **Fig. 9.** Geochemical, micropaleontologic and sedimentologic data for North Sea core 22/10a-4. (a)  
848 Lithologic formations, (b) bulk total organic carbon (TOC) isotopes, (c) carbon/nitrogen ratio, (d)  
849 dinoflagellate cysts tolerant of low salinity and high nutrients as percentage of all dinoflagellate  
850 cysts with known salinity preference, (e) percentage kaolinite (from Knox, 1996).

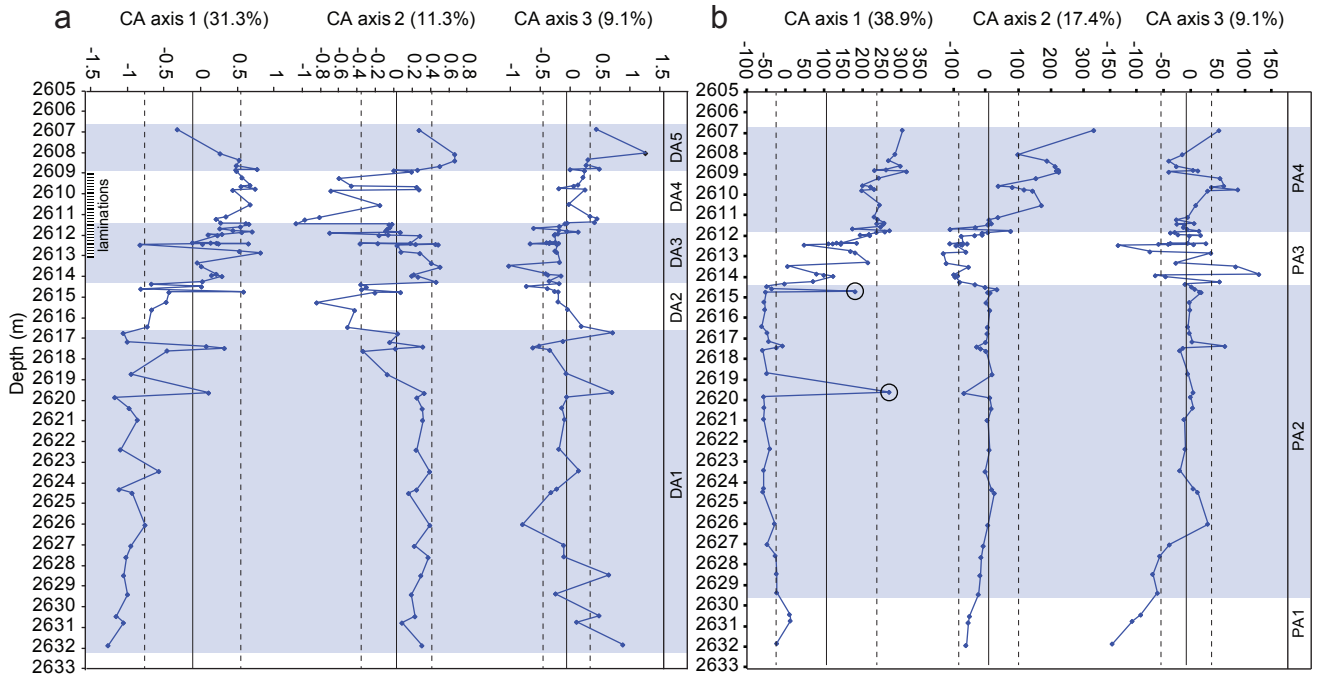
851

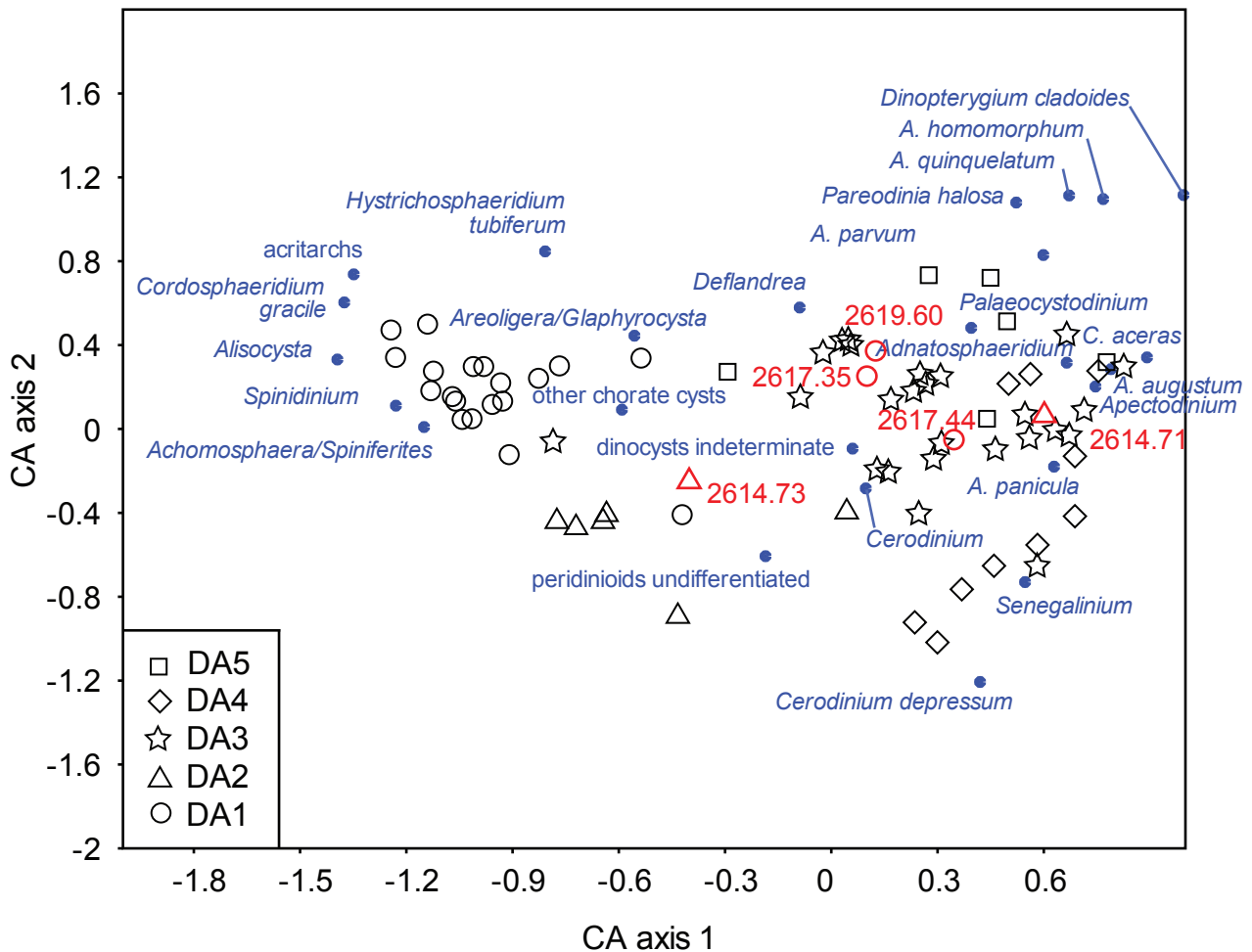
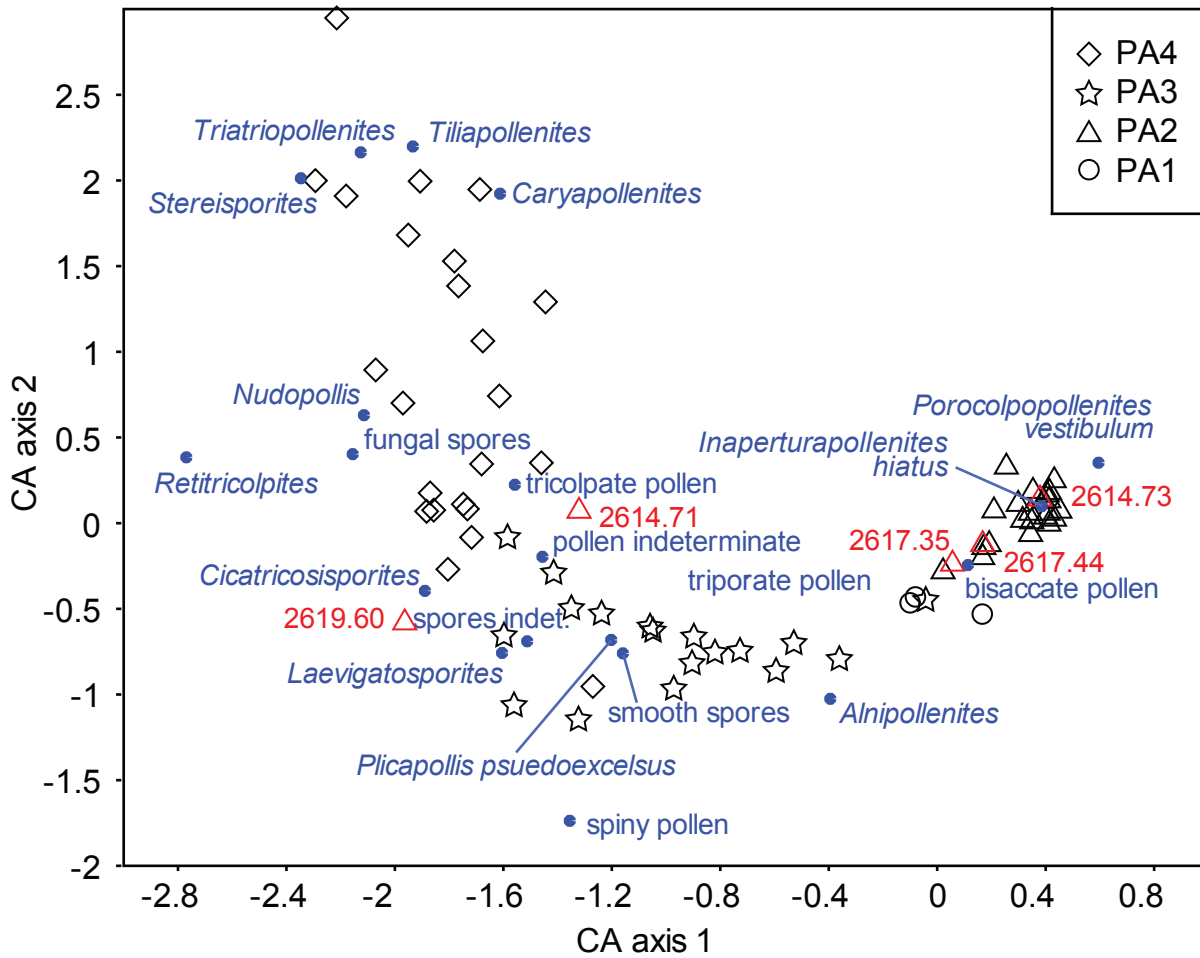
852 **Fig. 10.** Atomic C/N ratio distribution from all studied samples (Fig. S4). Shaded areas show  
853 typical values for modern algae and land plants (Meyers, 1997).

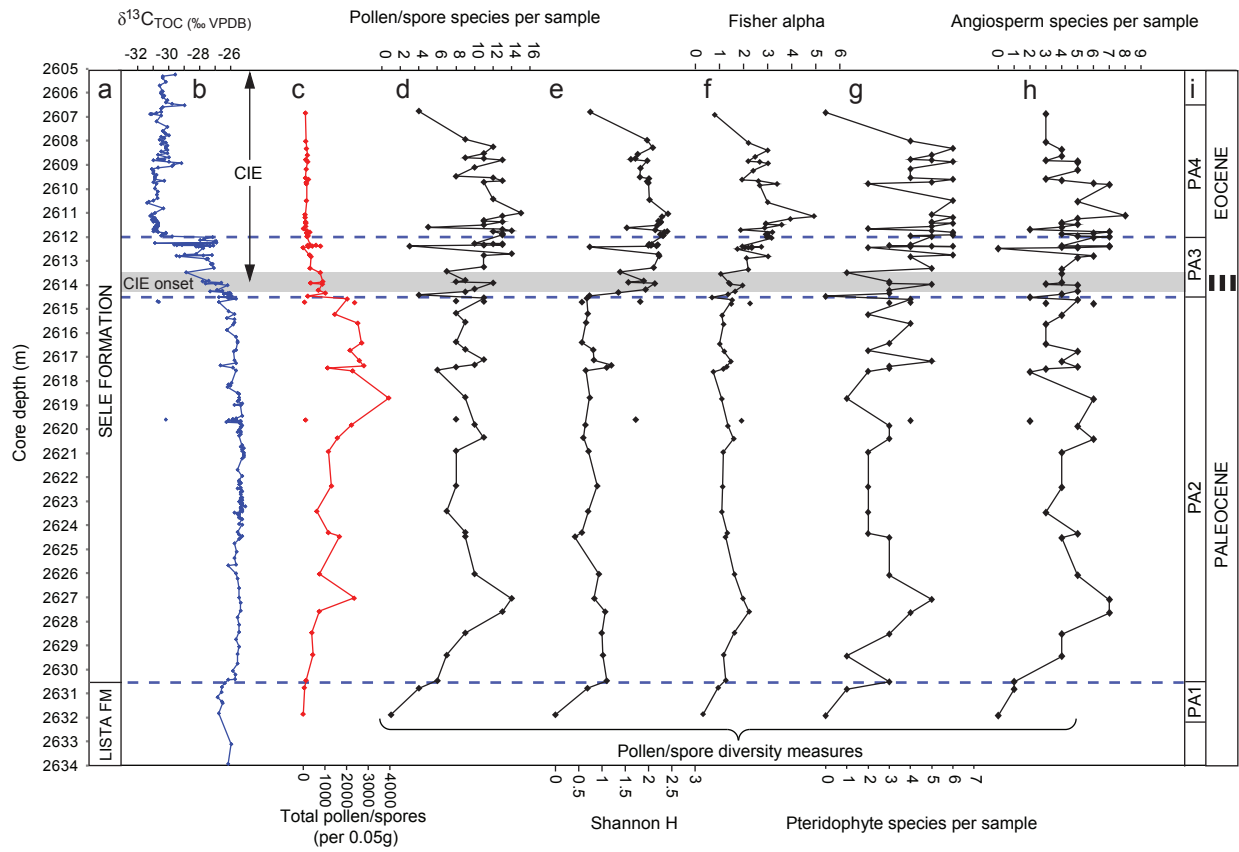


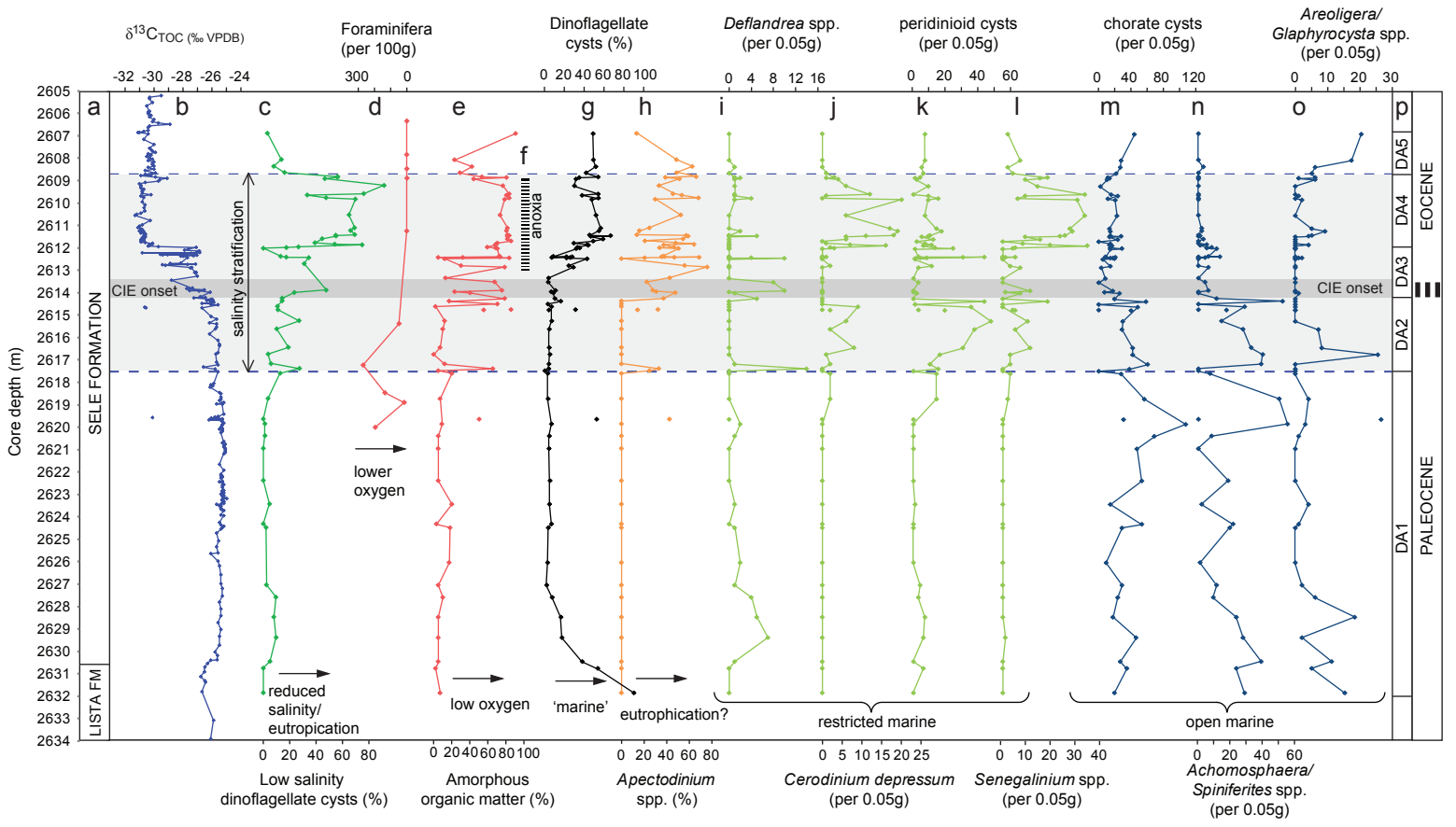


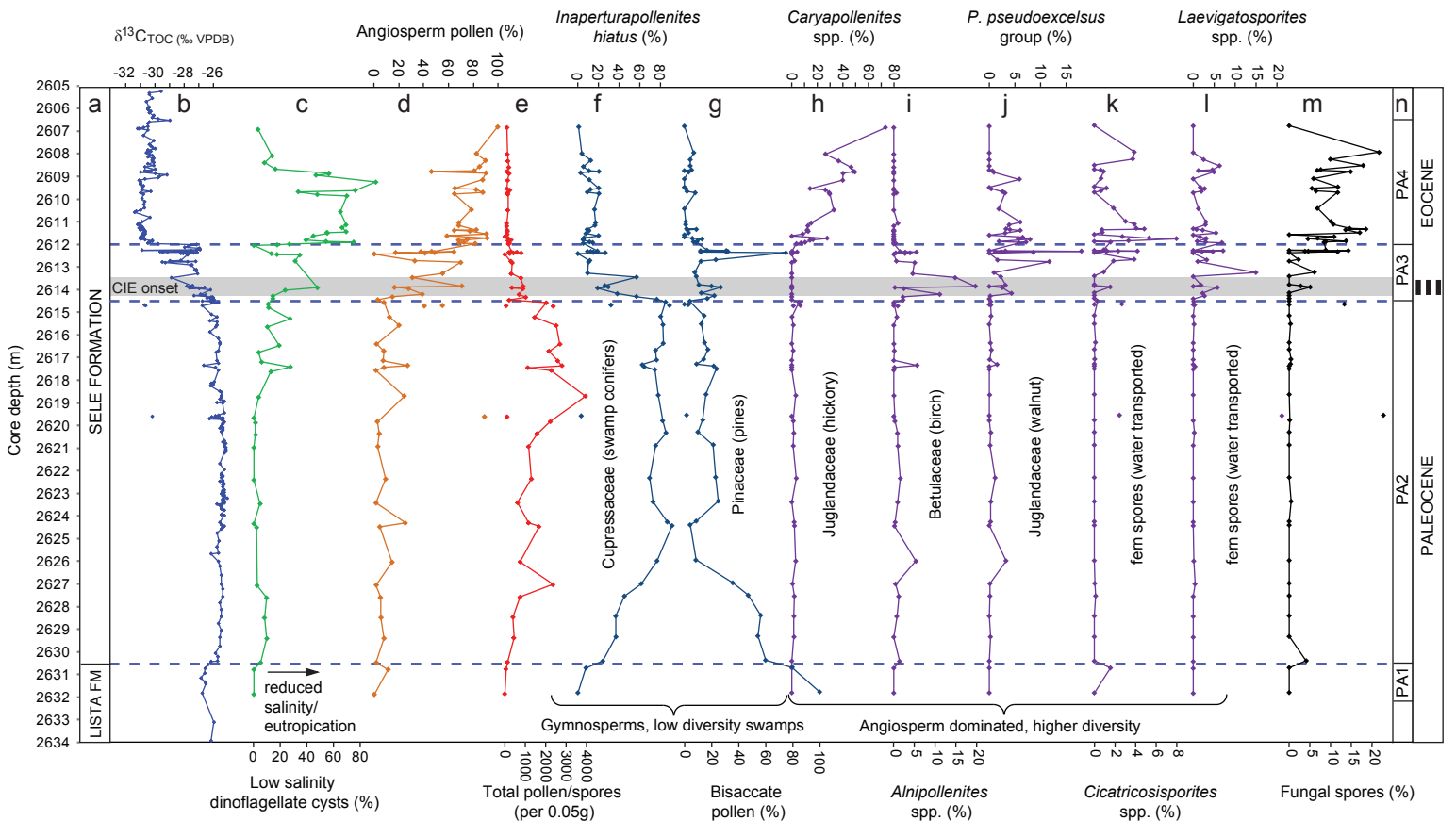


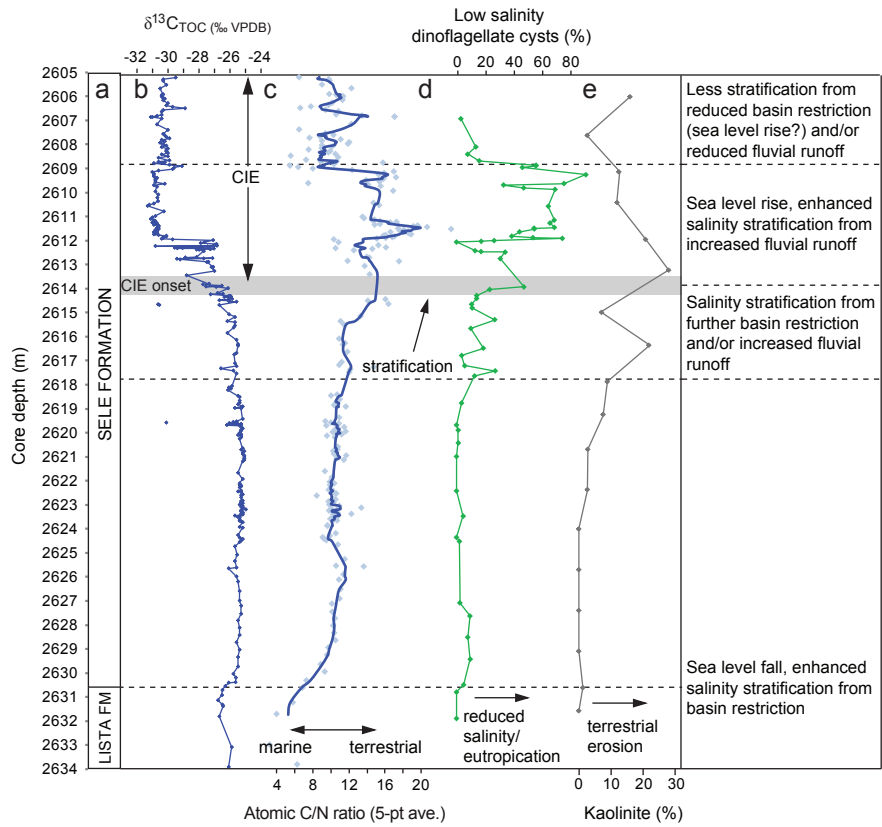


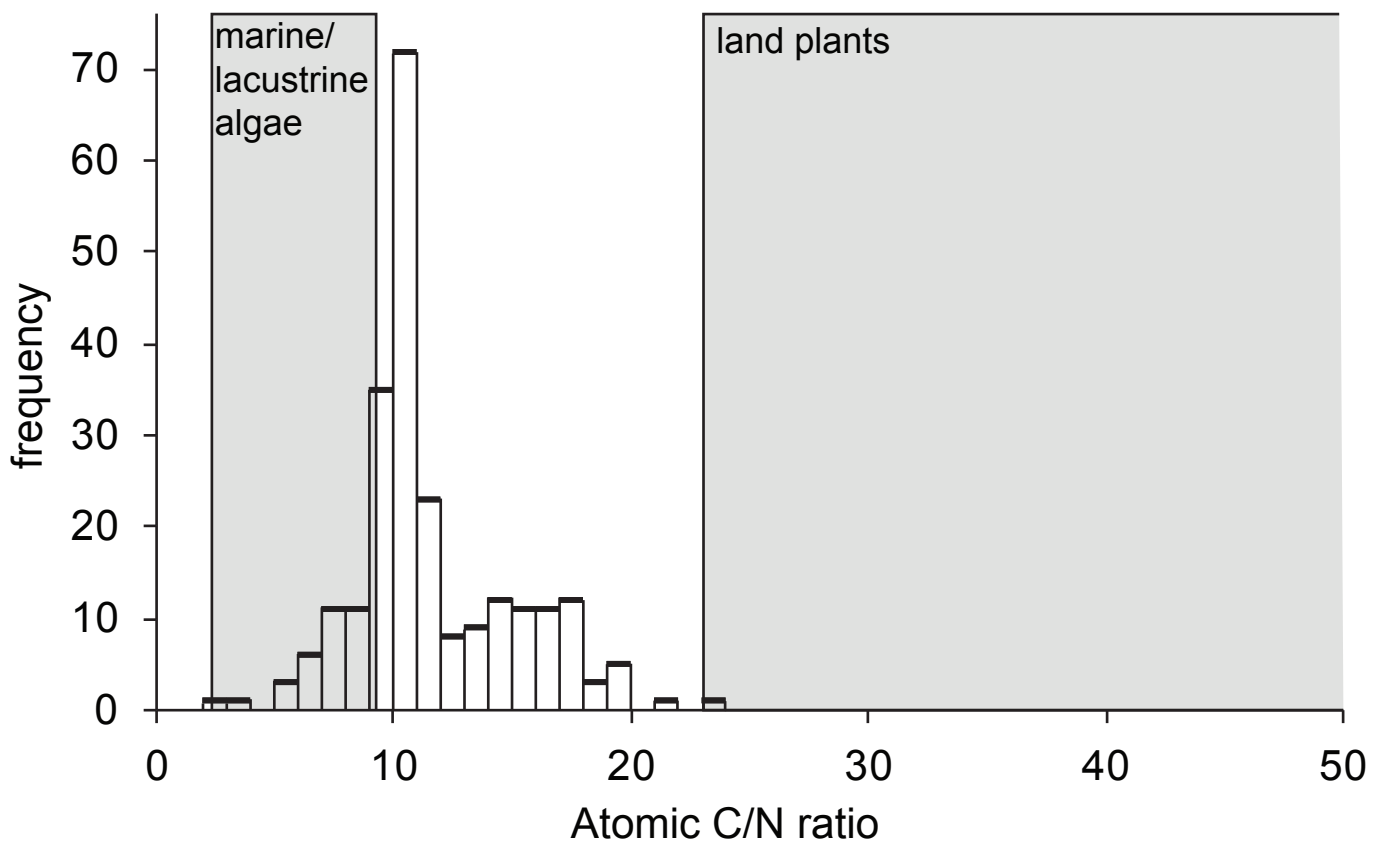












# 1 Marine and terrestrial environmental changes in NW Europe preceding carbon release 2 at the Paleocene-Eocene transition

3  
4 Supplementary Material

## 6 1. Isotope changes at the Paleocene-Eocene boundary

7  
8 Bulk sediment total organic carbon (TOC) isotopes ( $\delta^{13}\text{C}_{\text{TOC}}$ ) in core 22/10a-4 shift  
9 from consistently  $> -27\text{‰}$  to  $< -30\text{‰}$  within the interval  $\sim 2614$  to  $2612$  m core depth (Fig.  
10 3). The  $\sim 5\text{‰}$  excursion in  $\delta^{13}\text{C}_{\text{TOC}}$  is comparable in magnitude to organic carbon  $\delta^{13}\text{C}$  records  
11 of the PETM from the Lomonosov Ridge (Sluijs et al., 2006), Wilson Lake (Sluijs et al.,  
12 2007) and the North Sea (Sluijs et al., 2007), but larger than those from Spitsbergen (Harding  
13 et al., 2011) and Bass River (Sluijs et al., 2007). These differences in magnitude of the CIE  
14 may be partly due to simultaneous changes in proximal terrestrial vegetation type and/or  
15 shifts in marine plankton assemblages (Schouten et al., 2007; Handley et al., 2008). The first  
16 occurrence of the dinoflagellate marker species *Apectodinium augustum*, diagnostic of the  
17 Paleocene-Eocene boundary in the North Sea (Bujak and Brinkhuis, 1998; Sluijs et al., 2007),  
18 occurs in 22/10a-4 at  $\sim 2617$  m (Fig. 3).

19 In contrast to the low variability of  $\delta^{13}\text{C}_{\text{TOC}}$  preceding (SD =  $0.36\text{‰}$ , n = 106) and  
20 following (SD =  $0.52\text{‰}$ , n = 117) the onset of the CIE,  $\delta^{13}\text{C}_{\text{TOC}}$  values fluctuate by up to  $4\text{‰}$   
21 within the interval associated with the CIE onset at  $\sim 2614$  to  $2612$  m (dashed lines in Fig. 3).  
22 These  $\delta^{13}\text{C}_{\text{TOC}}$  fluctuations are not seen in other marginal marine records of the CIE (e.g.  
23 Harding et al., 2011), and are unlikely to be representative of the atmospheric carbon pool as  
24 the estimated speed of global carbon sequestration is too slow (Dickens et al., 1995; Bains et  
25 al., 2000; Zeebe et al., 2009). As the  $\delta^{13}\text{C}_{\text{TOC}}$  signature of organic carbon ( $\text{C}_{\text{org}}$ ) from the  
26 marine and terrestrial realms can be different, the fluctuations in  $\delta^{13}\text{C}_{\text{TOC}}$  observed at the  
27 onset of the CIE likely reflect varying contributions to  $\text{C}_{\text{org}}$  deposited within the North Sea  
28 Basin rather than changes within the global carbon system. The palynological results (from  
29 samples containing sufficient material for analysis; red symbols in Fig. 3) indeed show that  
30 %wood/plant tissue varies from 10% to 88% throughout this interval (Fig. S3). We found that  
31 the samples containing  $>30\%$  wood/plant tissue (empty red symbols in Fig. 3) in the  
32 palynological residues have consistently higher  $\delta^{13}\text{C}_{\text{TOC}}$  values than those with less  
33 wood/plant tissues (solid red symbols). These heavier values may indicate the presence of  
34 material reworked from older sediments with pre-CIE  $\delta^{13}\text{C}$  values, and if the hydrological

35 cycle was enhanced, excavation and re-deposition of latest Paleocene carbon might be  
36 expected. An equally valid alternate hypothesis is that they may partially reflect the high  
37 abundance of wood/plant tissue with potentially more positive  $\delta^{13}\text{C}_{\text{TOC}}$  values (terrestrial  
38 lignite deposit  $\delta^{13}\text{C}_{\text{TOC}}$  from southeast England ranged from  $-24.5\text{‰}$  before the CIE to  $-27\text{‰}$   
39 after the CIE, Collinson et al., 2007). Note here we are essentially arguing for more negative  
40 marine  $\delta^{13}\text{C}_{\text{TOC}}$  values than is typical for marine  $\text{C}_{\text{org}}$  (e.g. North Atlantic New Jersey Margin  
41  $-27\text{‰}$ , Sluijs et al., 2007). Usually Paleogene marine  $\text{C}_{\text{org}}$  exhibits similar or more positive  
42  $\delta^{13}\text{C}_{\text{TOC}}$  than terrestrial, but in the restricted North Sea (22/10a-4, see also Sluijs et al., 2007)  
43 a build up of nutrients may have lowered seawater  $\delta^{13}\text{C}$  to values below those typically found  
44 in the North Atlantic during the PETM – a hypothesis supported by  $\delta^{13}\text{C}_{\text{AOM}}$ , where AOM is  
45 probably of marine origin (see below). We note similarly low  $\delta^{13}\text{C}_{\text{TOC}}$  PETM values in  
46 marine sections from Spitsbergen (Harding et al., 2011) and the Lomonosov Ridge (Sluijs et  
47 al., 2006) – water masses linked to the restricted North Sea (Fig. 1). Restriction of the Arctic–  
48 Kilda–North Sea basins (Fig. 3) is also supported by laminations, marking anoxia at the CIE  
49 onset in all three sections from the North Sea (this study), Spitsbergen (Harding et al., 2011)  
50 and the Lomonosov Ridge (Sluijs et al., 2006). The presence of transported  $\text{C}_{\text{org}}$  thus  
51 precludes an unambiguous interpretation of the rate of atmospheric carbon release at the CIE  
52 onset, but the initial negative  $\delta^{13}\text{C}$  shift between 2614.3 and 2613.5 m (Fig. 3), which is  
53 especially pronounced in the  $\delta^{13}\text{C}_{\text{AOM}}$  data, can be taken as marking the earliest onset of the  
54 CIE.

55 A significant component of the palynological residues is amorphous organic matter  
56 (AOM), which becomes abundant during the CIE both in our records (Fig. 7e), and in Arctic  
57 Spitsbergen (Fig. 1, Harding et al., 2011). A marine origin for the AOM is indicated by  
58 evidence for enhanced primary productivity during the CIE, namely an increase in the  
59 abundance of low salinity tolerant dinoflagellate cysts, likely reflecting increased fluvial  
60 nutrient supply which would have stimulated primary productivity, and mm-scale laminations  
61 (Fig. 7f) reflecting anoxic bottom waters resulting from high fluxes of phytoplankton detritus.  
62 The %dinoflagellate cysts (compared to spores and pollen, Fig. 7g) also increases over the  
63 interval of increased AOM, indicating that the AOM is associated with an increase in marine  
64 dinoflagellate cysts and/or a reduction in terrestrial palynomorph input. The weak  
65 orange/brown fluorescence of the AOM is also typical of marine plankton-derived organic  
66 matter (Tyson, 1995; Omura and Hoyaagi, 2004; Harding et al., 2011), as is its association  
67 with abundant pyrite inclusions (Tyson, 1995). Carbon isotopic measurements of  
68 palynological residues dominated by AOM ( $\delta^{13}\text{C}_{\text{AOM}}$ , black symbols in Fig. 3) have lighter

69 values than  $\delta^{13}\text{C}_{\text{TOC}}$  in the majority of samples. If the AOM is of marine origin as we suggest,  
70 these lighter values appear to indicate that the North Sea was greatly enriched in  $^{12}\text{C}$   
71 compared to the New Jersey Shelf, North Atlantic ( $\delta^{13}\text{C}$  measured on marine dinoflagellate  
72 cysts, Sluijs et al., 2007), which ranged from  $-22\text{‰}$  before the CIE to  $-27\text{‰}$  after. This  
73 apparent  $-3.5\text{‰}$  offset between the North Sea and the North Atlantic could be due to the  
74 restricted nature of the North Sea Basin, with high productivity and apparent sluggish  
75 ventilation allowing the build-up of  $^{12}\text{C}$ , and/or a function of different fractionations between  
76 marine algae/bacteria (AOM) and dinoflagellate cysts. Although at a lower temporal  
77 resolution, the  $\delta^{13}\text{C}_{\text{AOM}}$  record (Fig. 3) supports  $\delta^{13}\text{C}_{\text{TOC}}$  positioning of the CIE onset at  
78  $\sim 2614$  m.

79

## 80 **2. Dinoflagellate paleoecology**

81

82 *Achomosphaera/Spiniferites* spp. was typically associated with open marine and  
83 hence normal marine salinity environments in the Paleogene of northern Italy (Brinkhuis,  
84 1994) and the New Jersey Shelf (Sluijs and Brinkhuis, 2009). Brinkhuis (1994) points out that  
85 the analogous extant *Spiniferites ramosus* is present in a wide variety of settings in both  
86 oceans and marginal seas (not specialised to restricted environments) but may be more  
87 prevalent in shelf areas. *Spiniferites* was also recorded in high abundance in marine PETM  
88 sediments in Spitsbergen (Harding et al., 2011) and interpreted as a distal marine influence.  
89 Undifferentiated chorate cysts, although unidentifiable to a species level, have a similar  
90 morphology and distribution to *Achomosphaera/Spiniferites* spp. (Fig. 7n) and may therefore  
91 have a similar, normal marine, ecologic signal.

92 *Areoligera/Glaphyrocysta* spp. were regarded as inhabiting inner neritic but not  
93 restricted localities (i.e. normal marine salinity) by Brinkhuis (1994), and are part of the un-  
94 restricted ‘coastal taxa’ of Pross and Brinkhuis (2005). *Achomosphaera/Spiniferites* spp. and  
95 *Areoligera/Glaphyrocysta* spp. are characteristic of the “*Hystriosphera* Association” and  
96 “*Areoligera* Association” from Paleogene sediments of Southeast England (Downie et al.,  
97 1971), suggested as representing open sea environments.

98 *Deflandrea* spp. was regarded as a coastal/neritic taxon indicating high productivity  
99 and nutrient availability (Brinkhuis, 1994; Pross and Brinkhuis, 2005), occurs in association  
100 with low salinity dinoflagellate cysts and freshwater algae in the Arctic (Sluijs et al., 2008),  
101 and was associated with biosiliceous horizons interpreted as high productivity in the North  
102 Atlantic (Firth, 1996).

103 *Cerodinium depressum* and *Senegalinium* spp. are both thought to tolerate very low  
104 salinity conditions based on their co-occurrence with terrestrial spores and pollen and  
105 freshwater algae (including *Botryococcus* and *Pediastrum*) in the Arctic (Brinkhuis et al.,  
106 2006; Sluijs et al., 2006; Sluijs et al., 2008). *Senegalinium* may also have been a  
107 heterotrophic genus indicative of elevated nutrient levels (Sluijs and Brinkhuis, 2009), and  
108 occurs during the PETM in the Southern Ocean (Sluijs et al., 2011) and Arctic Spitsbergen  
109 (Harding et al., 2011) in association with elevated levels of river-transported spores and  
110 pollen.

111 **Undifferentiated peridinoid cysts** ecology is less well constrained (and they are  
112 therefore not included in the %low salinity dinoflagellate cysts, Fig. 7c), they may also be  
113 indicative of elevated nutrient and reduced salinity conditions due to their similarity in form  
114 to other Paleogene peridinoids and the modern heterotrophic dinoflagellate *Protoperidinium*  
115 (Powell et al., 1992).

116 The migration of *Apectodinium* spp. from low to high latitudes during Paleocene-  
117 Eocene warming suggests a certain temperature control on its distribution (Bujak and  
118 Brinkhuis, 1998; Crouch et al., 2003b; Sluijs and Brinkhuis, 2009). An overriding  
119 temperature control on *Apectodinium* has been questioned however by (1) canonical  
120 correspondence analysis of sites at the New Jersey margin which show it correlated only  
121 weakly with temperature (Sluijs and Brinkhuis, 2009), (2) its occurrence in the Arctic at SSTs  
122 of only 23°C during the PETM (Sluijs et al., 2006), and (3) its pre-CIE peak in abundance in  
123 the Southern Ocean prior to any significant global warming (Sluijs et al., 2011). There is  
124 evidence that the occurrence of *Apectodinium* is associated with increased nutrient supply  
125 during the PETM, as it peaked in abundance coincident with periods of enhanced terrigenous  
126 input off New Zealand (Crouch et al., 2003a), elevated kaolinite percentages off Tunisia  
127 (Crouch et al., 2003b), peak runoff (terrestrially-derived matter) off Spitsbergen (Harding et  
128 al., 2011) and peak productivity (dinoflagellate cyst accumulation rates) on the New Jersey  
129 margin (Sluijs et al., 2007). An affinity for high nutrient supply is also consistent with the  
130 association of *Apectodinium* with elevated abundances of low salinity/high nutrient tolerant  
131 dinoflagellate cysts, increased terrigenous runoff (increased C/N ratio and kaolinite) in  
132 22/10a-4 (Fig. 9), although its occurrence does not precisely follow any one of these  
133 parameters. It has been suggested that *Apectodinium* did not thrive at very low salinities, as it  
134 was outcompeted by low salinity dinoflagellate cysts in the Arctic Ocean (Sluijs et al., 2006;  
135 2007), and does not always follow the abundance patterns of low salinity tolerant  
136 dinoflagellate cysts in 22/10a-4 (Fig. 7c) or the New Jersey margin (Sluijs et al., 2007).

137 Although no single environmental condition could be responsible for the *Apectodinium* acme  
138 during the PETM in so many diverse environments (Crouch et al., 2003b; Sluijs et al., 2007),  
139 warming before and during the PETM may have opened the corridor for its migration and  
140 invasion of higher latitudes (Crouch et al., 2003b), where it appears to have outcompeted  
141 existing species that may have been less well adapted. Due to the sporadic migration of  
142 *Apectodinium* over the PETM, it may not be possible to use this species as a faithful indicator  
143 for specific environmental conditions at higher latitudes.

144

### 145 **3. Foraminifera**

146

147 Ten samples were analysed for foraminifera (Fig. 7d) in order to characterise benthic  
148 conditions. Abundant and low diversity assemblages were recovered between ~2620 and  
149 2615 m (Table S2), containing an average of 130 specimens/g of dried sediment, and nine  
150 species of benthic foraminifera were recovered in total. These samples were dominated by  
151 *Haplophragmoides walteri* and *Hyperammina* spp., and all species observed are agglutinated  
152 non-calcareous forms. It is possible that calcareous species were never present in the central  
153 North Sea at this time, or that secondary dissolution has preferentially removed these forms.  
154 This low diversity, non-calcareous, agglutinated fauna is indicative of low oxygen marine  
155 environments (Gradstein and Berggren, 1981; Charnock and Jones, 1990; Gradstein et al.,  
156 1992). Samples from the interval ~2611 to 2606 m associated with full PETM conditions and  
157 the upper part of the laminated section, are found to be barren of all foraminifera including a  
158 near absence of foraminiferal test linings in the palynological residues (Table S1). The lack  
159 of benthic foraminifera within the laminated sediments is consistent with the interpretation of  
160 anoxic bottom water.

161

### 162 **References**

163

- 164 Bains, S., Norris, R.D., Corfield, R.M., Faul, K.L., 2000. Termination of global warmth at the  
165 Palaeocene/Eocene boundary through productivity feedback. *Nature* 407, 171–174.
- 166 Brinkhuis, H., 1994. Late Eocene to early Oligocene dinoflagellate cysts from the Priabonian  
167 tye area (northeast Italy); biostratigraphy and palaeoenvironmental interpretation.  
168 *Palaeogeogr. Palaeoclimatol. Palaeoecol.* 107, 121–163.
- 169 Brinkhuis, H., Schouten, S., Collinson, M.E., Sluijs, A., Sinninghe Damsté, J.S., Dickens,  
170 G.R., Huber, M., Cronin, T.M., Jonaotaro Onodera, J., Takahashi, K., Bujak, J.P., Stein,

171 R., van der Burgh, J., Eldrett, J.S., Harding, I.C., Lotter, A.F., Sangiorgi, F., Cittert, H.,  
172 de Leeuw, J.W., Matthiessen, J., Backman, J., Moran, K., the Expedition 302 Scientists,  
173 2006. Episodic fresh surface waters in the Eocene Arctic Ocean. *Nature* 441, 606–609.

174 Bujak, J., Brinkhuis, H., 1998. Global Warming and Dinocyst Changes across the  
175 Palaeocene/Eocene Epoch Boundary. In: Aubry, M.-P., Lucas, S.G., Berggren, W.A.  
176 (Eds.), *Late Palaeocene–Early Eocene Biotic and Climatic Events in Marine and*  
177 *Terrestrial Records*. Columbia Univ. Press, New York, pp. 277–295.

178 Charnock, M.A., Jones, R.W. 1990. Agglutinated foraminifera from the Palaeogene of the  
179 North Sea. In: Hemleben, C., Kaminski, M.A., Kuhnt, W., Scott, D.B. (Eds.),  
180 *Paleoecology, Biostratigraphy, Paleoceanography and Taxonomy of Agglutinated*  
181 *Foraminifera*. NATO Advanced Study Institutes, Series C 327, pp. 139–244.

182 Collinson, M.E., Steart, D.C., Scott, A.C., Glasspool, I.J., Hooker, J.J., 2007. Episodic fire,  
183 runoff and deposition at the Palaeocene-Eocene boundary. *J. Geol. Soc. Lond.* 164, 87–  
184 97.

185 Coward, M.P., Dewey, J., Hempton, M., Holroy, J., 2003. Tectonic evolution. In: Evans, D.,  
186 Graham, C., Armour, A., Bathurst, P., *The Millennium Atlas; Petroleum Geology of the*  
187 *Central and Northern North Sea* (Eds.) Geological Society, London pp. 17–33.

188 Crouch, E.M., Dickens, G.R., Brinkhuis, H., Aubry, M., Hollis, C.J., Rogers, K.M., Visscher,  
189 H., 2003a. The Apectodinium acme and terrestrial discharge during the Paleocene–  
190 Eocene Thermal Maximum: new palynological, geochemical and calcareous  
191 nannoplankton observations at Tawanui, New Zealand. *Palaeogeogr. Palaeoclimatol.*  
192 *Palaeoecol.* 194, 387–403.

193 Crouch, E.M., Brinkhuis, H., Visscher, H., Adatte, H., Bolle, M.–P., 2003b. Late  
194 Palaeocene–early Eocene Dinoflagellate Cyst Records from the Tethys; Further  
195 Observations on the Global Distribution of Apectodinium. In: Wing, S., Gingerich, P.D.,  
196 Schmitz, B., Thomas, E. (Eds.), *Causes and Consequences of Globally Warm Climates*  
197 *in the Early Paleogene: Geol. Soc. Am. Spec. Pap.*, vol. 369. Geological Society of  
198 America Inc., Boulder, Colorado, pp. 113–131.

199 Dickens, G.R., O’Neil, J.R., Rea, D.K., Owen, R.M., 1995. Dissociation of oceanic methane  
200 hydrate as a cause of the carbon isotope excursion at the end of the Paleocene.  
201 *Paleoceanography* 10, 965–971.

202 Downie, C., Hussain, M.A., Williams, G.L., 1971. Dinoflagellate cyst and acritarch  
203 associations in the Paleogene of Southeast England. *Geoscience and Man* 3, 29–35.

204 Firth, J.V., 1996. Upper middle Eocene to Oligocene dinoflagellate biostratigraphy and  
205 assemblage variations in hole 913B, Greenland Sea. In: Thiede, J., Myrhe, A.M., Firth,  
206 J.V., Johnson, G.L., Ruddiman, W.F. (Eds.), Proceedings of the Ocean Drilling Program.  
207 Scientific Results, pp. 203– 242.

208 Gradstein, F.M., Berggren, W.A., 1981. Flysch-type agglutinated foraminifera and the  
209 Maestrichtian to Paleogene history of the Labrador and North Sea. *Marine*  
210 *Micropaleontology* 6, 211-268.

211 Gradstein, F.M., Kristiansen, I.L., Loemo, L., Kaminski, M.A., 1992. Cenozoic foraminiferal  
212 and dinoflagellate cyst biostratigraphy of the Central North Sea. *Micropaleontology* 38,  
213 101-137.

214 Handley, L., Pearson, P.N., McMillan, I.K., Pancost, R.D., 2008. Large terrestrial and marine  
215 carbon and hydrogen isotope excursions in a new Paleocene/Eocene boundary section  
216 from Tanzania. *Earth Planet. Sci. Lett.* **275**, 17-25.

217 Hammer, Ø, Harper, D., Ryan, P.D., 2005. PAST: Palaeontological statistics software  
218 package for education and data analysis. *Palaeontologia Electronica* 4, pp. 9. Harding et  
219 al., 2011

220 Harding, I.C., Charles, A.J., Marshall, J.E.A., Pälike, H., Roberts, A.P., Wilson, P.A., Jarvis,  
221 E., Thorne, R., Morris, E., Moremon, R., Pearce, R.B., Akbari, S., 2011. Sea-level and  
222 salinity fluctuations during the Paleocene-Eocene thermal maximum in Arctic  
223 Spitsbergen. *Earth Planet. Sci. Lett.* 303, 97-107.

224 Omura, A., Hoyanagi, K., 2004. Relationships between composition of organic matter,  
225 depositional environments, and sea level changes in backarc basins, Central Japan.  
226 *Journal of Sedimentary Research* 74, 620-630.

227 Powell, A.J., Lewis, J., Dodge, J.D., 1992. A palynological expression of post-Palaeogene  
228 upwelling: a review. In: Prell, C.P., Emeis, K.C. (Eds.), *Upwelling systems: Evolution*  
229 *since the Early Miocene*. Special Publication, vol. 64. Geological Society of London, pp.  
230 215-226.

231 Pross, J., Brinkhuis, H., 2005. Organic-walled dinoflagellate cysts as paleoenvironmental  
232 indicators in the Paleogene; a synopsis of concepts. *Paläontologische Zeitschrift* 79, 53-  
233 59.

234 Schouten, S., Woltering, M., Rijpstra, I.C., Sluijs, A., Brikhuis, H., Sinninghe Damsté, J.S.,  
235 2007. The Paleocene–Eocene carbon isotope excursion in higher plant organic matter:  
236 differential fractionation of angiosperms and conifers in the Arctic. *Earth Planet. Sci.*  
237 *Lett.* 258, 581–592.

- 238 Sluijs, A., Brinkhuis, H., 2009. A dynamic climate and ecosystem state during the Paleocene–  
239 Eocene Thermal Maximum: inferences from dinoflagellate cyst assemblages on the New  
240 Jersey Shelf. *Biogeosciences* 6, 1755–1781.
- 241 Sluijs, A., Schouten, S., Pagani, M., Woltering, M., Brinkhuis, H., Sinninghe Damsté, J.S.,  
242 Dickens, G.R., Huber, M., Reichart, G.J., Stein, R., Matthiessen, J., Lourens, L.J.,  
243 Pedentchouk, N., Backman, J., Moran, K., Expedition 302 Scientists, 2006. Subtropical  
244 Arctic Ocean temperatures during the Palaeocene–Eocene Thermal Maximum. *Nature*  
245 441, 610–613.
- 246 Sluijs, A., Brinkhuis, H., Schouten, S., Bohaty, S.M., John, C.M., Zachos, J.C., Reichart, G.,  
247 Sinninghe Damsté, J.S., Crouch, E.M., Dickens, G.R., 2007. Environmental precursors to  
248 light carbon input at the Paleocene/Eocene boundary. *Nature* 450, 1218-1221.
- 249 Sluijs, A., Röhl, U., Schouten, S., Brumsack, H., Sangiorgi, F., Sinninghe Damsté, J.S.,  
250 Brinkhuis, H., 2008. Arctic late Paleocene-early Eocene paleoenvironments with special  
251 emphasis on the Paleocene-Eocene thermal maximum (Lomonosov Ridge, Integrated  
252 Ocean Drilling Program Expedition 302). *Paleoceanography* 23, PA1S11,  
253 doi:10.1029/2007PA001495.
- 254 Sluijs, A., Bijl, P.K., Schouten, S., Röhl, U., Reichart, G.-J., Brinkhuis, H., 2011. Southern  
255 ocean warming, sea level and hydrological change during the Paleocene-Eocene thermal  
256 maximum. *Climate of the Past* 7, 47-61.
- 257 Tyson, R.V. 1995. *Sedimentary Organic Matter: Organic Facies and Palynofacies*. Chapman  
258 and Hall, London, pp. 615.
- 259 Zeebe, R.E., Zachos, J.C., Dickens, G.R., 2009. Carbon dioxide forcing alone insufficient to  
260 explain Palaeocene-Eocene Thermal Maximum warming. *Nature Geosci.* 2, 576-580.

261

## 262 **Supplementary tables**

263

264 **Table S1.** Raw counts (apart from \*) of palynomorphs from 22/10a-4. All specimens on a  
265 single slide were counted. As each slide was made with 0.05 g of sediment, all counts  
266 represent specimens/0.05 g. \* = Estimate of total specimens per slide (specimens/0.05 g),  
267 these specimens counted to >300, and subsequently scaled up to an estimate for the whole  
268 slide by number of traverses taken.

269

270 **Table S2.** Raw counts of benthic foraminifera from 22/10a-4.

271

272 **Table S3.** C and N wt% data from 22/10a-4.

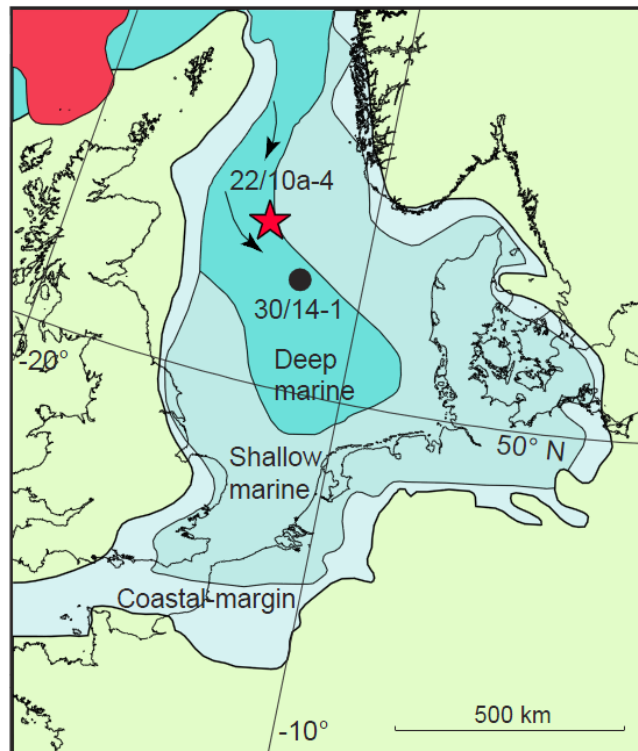
273

274 **Table S4.** Carbon isotope data from 22/10a-4.

275

276 **Supplementary figures**

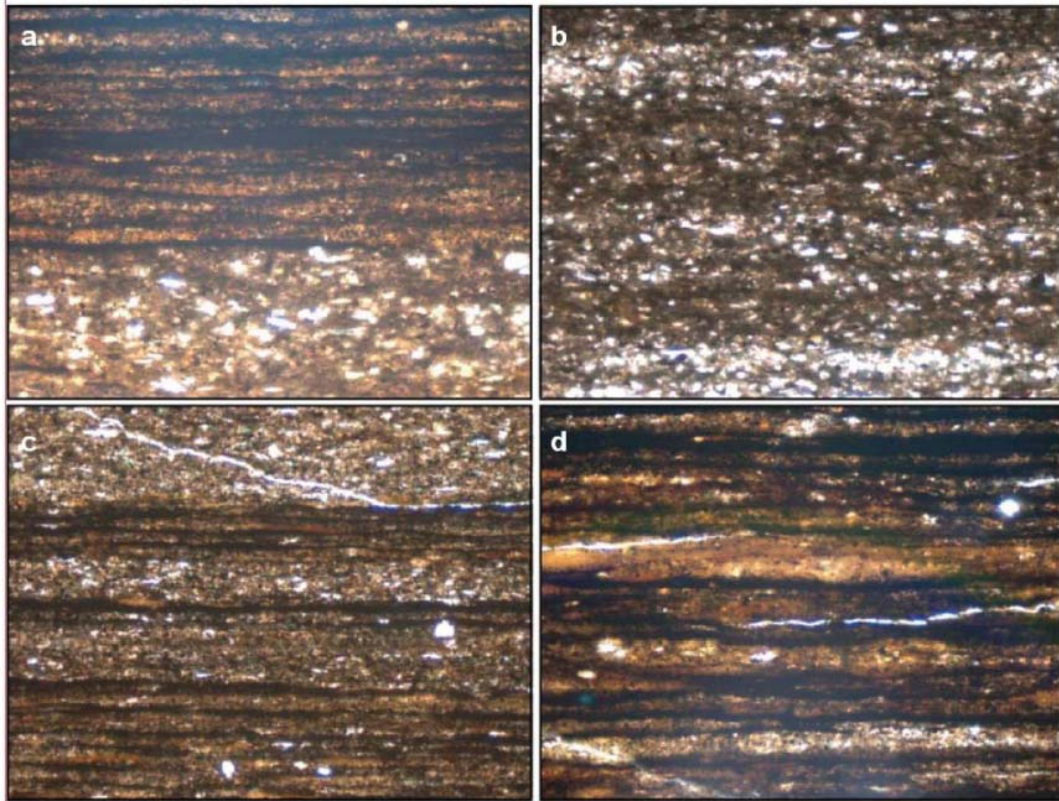
277



278

279

280 **Fig. S1.** Paleogeographic reconstruction of the North Sea area for the Paleocene/Eocene at  
281 ~55.5 Ma (Coward et al., 2003), with locations of cores 22/10a-4 (this study, 57°44'8.47''N.  
282 1°50'26.59''E.) and 30/14-1 (Sluijs et al., 2007). Arrows indicate principal direction of  
283 sediment flow, red is area of basaltic volcanism, deep marine equates to middle bathyal (500-  
284 1000 m water depth).



285

286

287

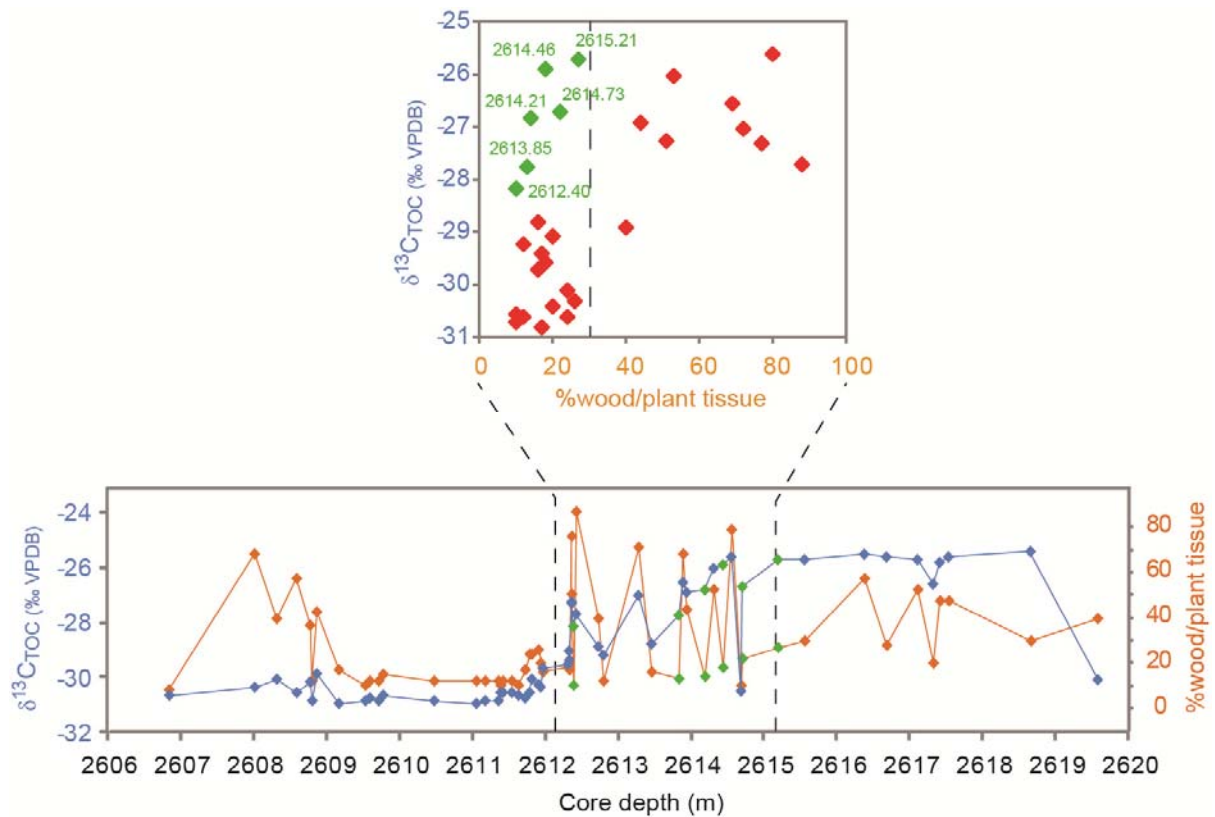
288

289

290

291

**Fig. S2.** Transmitted light microscope images of thin sections from core 22/10a-4 from 4 horizons. (a) 2612.266 mbsf, (b) 2612.226 mbsf, (c) 2612.176 mbsf, and (d) 2611.986 mbsf. Laminations are laterally continuous and vary in thickness. Dark laminae are organic rich, light laminae are clay and sand rich. An average of ~13 laminae per mm occur throughout the section. Scale bar = 0.5 mm.



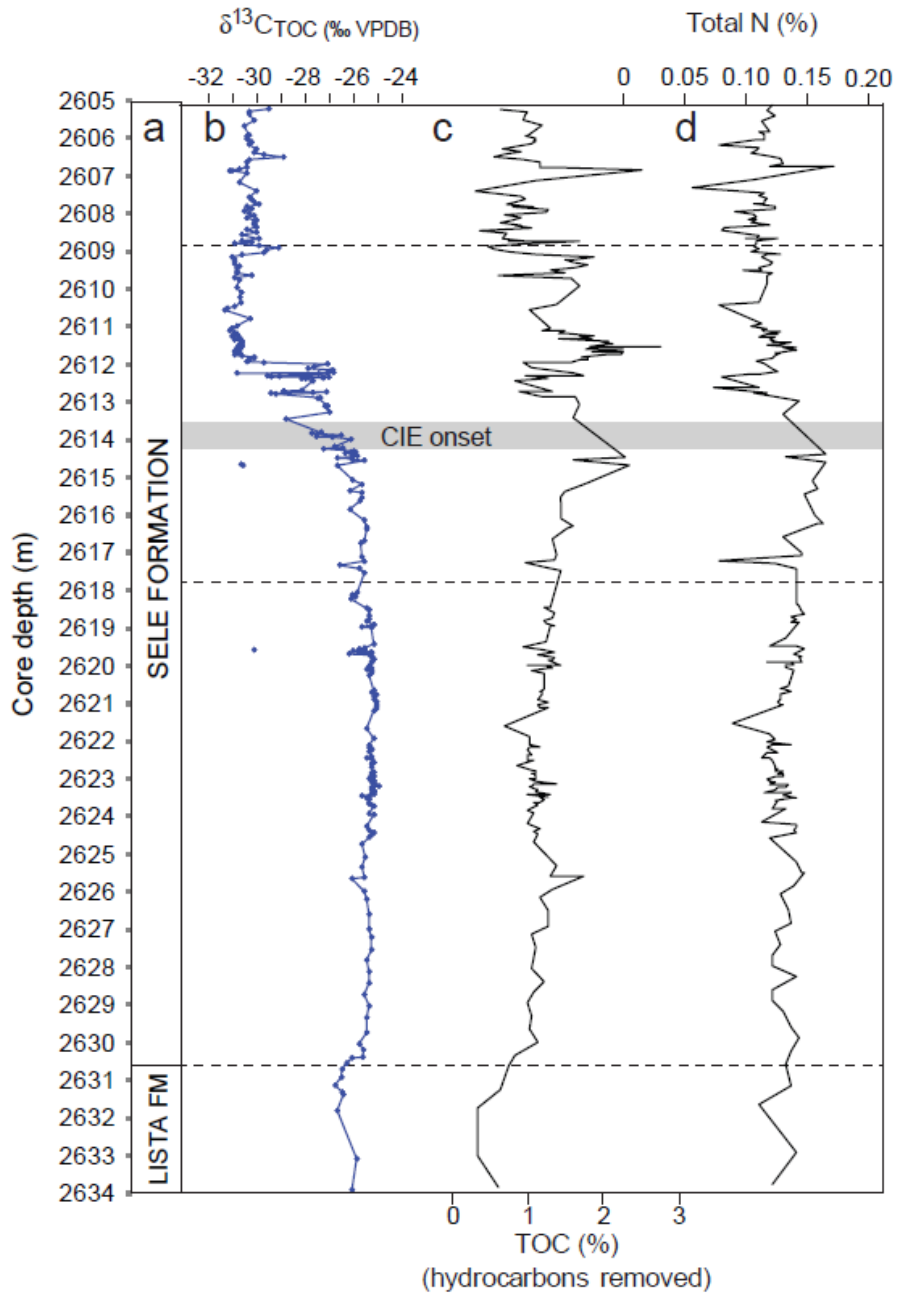
292

293

294 **Fig. S3.** Core 22/10a-4 %wood/plant tissues (from all palynological residues) plotted with  
 295 their corresponding bulk carbon isotopes ( $\delta^{13}\text{C}_{\text{TOC}}$ ). All samples with >30% wood/plant tissue  
 296 within the CIE (~2615-2612 m) exhibit heavier  $\delta^{13}\text{C}_{\text{TOC}}$  values (upper plot) uncharacteristic  
 297 of PETM values, signifying either re-deposited pre-CIE terrestrial material and/or transported  
 298 terrestrial material with more positive  $\delta^{13}\text{C}_{\text{TOC}}$  values than contemporaneous North Sea  
 299 marine organic carbon. Positive  $\delta^{13}\text{C}_{\text{TOC}}$  samples within the CIE onset that do not have >30%  
 300 wood/plant tissue are marked in green. The majority fall within the early CIE onset as  
 301 expected. One sample at 2612.40 m however has relatively high  $\delta^{13}\text{C}_{\text{TOC}}$ . As there is <30%  
 302 wood/plant tissue in this sample, it is possible that it represents a pulse of non-woody  
 303 terrestrial material transported to 22/10a-4, possibly peat.

304

305



306

307

308 **Fig. S4.** Total organic carbon (TOC) and total nitrogen (TN) wt% values for 22/10a-4.